JOURNAL OF VIROLOGY, Oct. 2010, p. 10888–10906 Vol. 84, No. 20
0022-538X/10/$12.00 doi:10.1128/JVI.00431-10

Quantitative Proteomic Analyses of Influenza Virus-Infected Cultured Human Lung Cells▽†

Kevin M. Coombs,[1,2,3]* Alicia Berard,[1,2] Wanhong Xu,[1,2] Oleg Krokhin,[2] Xiaobo Meng,[2] John P. Cortens,[2] Darwyn Kobasa,[1,4] John Wilkins,[2,5] and Earl G. Brown[6]

Department of Medical Microbiology, Faculty of Medicine, University of Manitoba, Winnipeg, Manitoba R3E 0J6, Canada[1]; Manitoba Centre for Proteomics & Systems Biology, Room 799, 715 McDermot Avenue, Winnipeg, Manitoba R3E 3P4, Canada[2]; Manitoba Institute of Child Health, Room 513, John Buhler Research Centre, 715 McDermot Avenue, Winnipeg, Manitoba R3E 3P4, Canada[3]; Respiratory Viruses Program, National Microbiology Laboratory, Public Health Agency of Canada, Winnipeg, Manitoba R3E 3R2, Canada[4]; Department of Internal Medicine, Faculty of Medicine, University of Manitoba, Winnipeg R3E 3P4, Canada[5]; and Department of Biochemistry, Microbiology, and Immunology, and Emerging Pathogens Research Centre, University of Ottawa, Ottawa, Ontario K1H 8M5, Canada[6]

Received 26 February 2010/Accepted 30 July 2010

Because they are obligate intracellular parasites, all viruses are exclusively and intimately dependent upon host cells for replication. Viruses, in turn, induce profound changes within cells, including apoptosis, morphological changes, and activation of signaling pathways. Many of these alterations have been analyzed by gene arrays, which measure the cellular "transcriptome." Until recently, it has not been possible to extend comparable types of studies to globally examine all the host cellular proteins, which are the actual effector molecules. We have used stable isotope labeling by amino acids in cell culture (SILAC), combined with high-throughput two-dimensional (2-D) high-performance liquid chromatography (HPLC)/mass spectrometry, to determine quantitative differences in host proteins after infection of human lung A549 cells with human influenza virus A/PR/8/34 (H1N1) for 24 h. Of the 4,689 identified and measured cytosolic protein pairs, 127 were significantly upregulated at >95% confidence, 153 were significantly downregulated at >95% confidence, and a total of 87 proteins were upregulated or downregulated more than 5-fold at >99% confidence. Gene ontology and pathway analyses indicated differentially regulated proteins and included those involved in host cell immunity and antigen presentation, cell adhesion, metabolism, protein function, signal transduction, and transcription pathways.

Influenza A virus (FLUAV), a member of the family *Orthomyxoviridae*, is a small enveloped virus with a genome consisting of 8 segments of negative-sense single-stranded RNA that encodes for 10 to 11 proteins depending on the strain (56). The segmented genome and highly error-prone viral replication lead to enormous genetic plasticity, mediated by nucleotide or genome segment exchange, termed genetic drift or genetic shift, respectively. Genomic changes control the differences in virulence and host range seen among FLUAV isolates. FLUAVs are serologically categorized by 2 surface proteins: hemagglutinin (HA), of which there are currently 16 types (H1 to H16), and neuraminidase (NA), of which there are currently 9 types (N1 to N9) (56). Virtually every possible H-N combination has been found in water fowl (2, 46), the generally accepted reservoir, but only a few H-N types have circulated in humans: H1N1 (1918 "Spanish Flu" and the current pandemic H1N1 2009 strains), H2N2, and H3N2. A number of antiviral strategies, including vaccines and small molecule inhibitors, have been developed to combat this virus, but its genetic plasticity often leads to resistance to virus-targeted antiviral strategies. Because of its small genome, the virus, like other viruses, is an obligate parasite and must make extensive use of host cell machinery. Thus, an alternate antiviral strategy could be to better understand the critical host factors that are influenced and required by the virus for its efficient propagation.

While a cell's genome generally remains relatively constant (except for certain epigenetic events; see references 28 and 33 for reviews), the cell's proteome (the total protein repertoire, including how any given protein may be cotranslationally or posttranslationally modified) varies greatly due to its biochemical interactions with the genome, as well as the cell's interactions with the environment. A cell's protein expression is dependent on the location of the cell, different stages of its life cycle, and different environmental conditions. In the case of viruses, which require the host cell's machinery and metabolism to replicate, the cell's proteome also reflects the specific alterations of the pathways induced by virus infection.

Previous analyses of how cells respond to influenza virus infection have used microarray technologies which measure the cellular "transcriptome" (for examples, see references 6, 30, and 45). However, there frequently is little concordance between microarray and protein data (6, 52, 71), partly because mRNA levels cannot provide complete information about lev-

* Corresponding author. Mailing address: Manitoba Centre for Proteomics and Systems Biology, Room 799 John Buhler Research Centre, 715 McDermot Avenue, Winnipeg, MB R3E 3P4, Canada. Phone: (204) 789-3976. Fax: (204) 480-1362. E-mail: kcoombs@cc.umanitoba.ca.

† Supplemental material for this article may be found at http://jvi.asm.org/.

▽ Published ahead of print on 11 August 2010.

els of protein synthesis or extents of posttranslational modifications. Thus, proteomic analyses have also been employed to better understand host alterations to virus infection. Vester et al. used two-dimensional difference in gel electrophoresis (2-D DIGE) and identified 8 significantly altered host proteins in influenza virus A/PR/8/34 (H1N1)-infected MDCK and human A549 cells (72), and Liu and colleagues used a similar approach to identify about 25 significantly altered host proteins in avian influenza A/Hong Kong/108/2003 (H9N2)-infected human gastric carcinoma cells (48).

There have been a number of significant improvements in quantitative proteomic analyses, particularly in areas of non-gel-based studies, such as isotope-coded affinity tags (ICAT) (see references 11, 35, and 39 for some examples), isobaric tags for relative and absolute quantitation (iTRAQ) (see references 12, 20, 61, and 77 for examples), and stable isotope labeling by amino acids in cell culture (SILAC) (see references 15, 16, 27, 34, and 55 for examples). There also have been improvements in peptide fractionation (22, 67). Therefore, we decided to apply newer quantitative approaches to more fully probe the richness of influenza virus-infected host cell proteomes to attempt to identify additional potential antiviral targets. We chose SILAC, using $^{12}C_6$-Lys and $^{12}C_6{}^{14}N_4$-Arg ("light" [L]) and $^{13}C_6$-Lys and $^{13}C_6{}^{15}N_4$-Arg ("heavy" [H]), because virtually every tryptic peptide is expected to contain an L or H label, thereby providing increased protein coverage; L and H samples are mixed together early in the process, thereby reducing sample-to-sample variability, and other such studies succeeded in identifying and quantitatively measuring up to several thousand proteins (7, 15, 34, 62). We succeeded in the current study in identifying and measuring nearly 4,700 cytosolic host proteins, of which 127 were significantly upregulated, including proteins involved in acetylation, cell structure, defense responses, protein binding, and responses to stress, stimulus, and virus, and 153 proteins, including those involved in alternative splicing, localization, transport, protein binding, and nucleoside, nucleotide, and nucleic acid metabolism that were significantly downregulated.

MATERIALS AND METHODS

Cells and viruses. (i) Viruses. Influenza virus strain A/PR/8/34 (H1N1) was grown in embryonated hen eggs from laboratory stocks, and chorioallantoic fluid was harvested, aliquoted, and titered in MDCK cells by standard procedures (8). Additional stocks were made by recombinant means to exclude chorioallantoic fluid effects (53).

(ii) Cells. Human lung A549 cells were routinely cultured in Dulbecco's modified Eagle's medium (DMEM) supplemented with nonessential amino acids, sodium pyruvate, 0.2% (wt/vol) glucose, 10% fetal bovine serum (FBS; Intergen), and 2 mM L-glutamine. Cells were maintained as monolayers in 10% CO_2 and were passaged by trypsinization 2 to 3 times each week. For SILAC labeling, cells were grown in DMEM provided with a SILAC phosphoprotein identification and quantification kit (Invitrogen Canada Inc.; Burlington, Ontario, Canada), supplemented as above (except without nonessential amino acids), and with 10% dialyzed FBS (Invitrogen Canada Inc.; Burlington, Ontario, Canada) plus 100 mg each of "light" (L) or "heavy" (H) L-lysine and L-arginine per liter of DMEM.

Infection. Once the cells had grown through six doublings, L cells in T25 and T75 flasks were infected with A/PR/8/34 at a multiplicity of infection (MOI) of 7 PFU per cell. An equivalent number of H cells were mock infected as the control. Cells were overlaid with the appropriate medium and cultured for various periods of time. Infections were carried out multiple times over several months.

Photomicrography. Infected and mock-infected cells in the T25 flask were examined microscopically for cytopathic effect (CPE) at 0, 12, 18, 24, 30, and 36 h postinfection with a Nikon TE-2000, and cells were photographed with a Canon-A700 digital camera. Images were imported into Adobe and slight adjustments made in brightness and contrast, which did not alter image context with respect to each other.

Cell fractionation. At 24 h postinfection, L and H cells in the T75 flasks were collected and counted. To verify the infection status of each culture, aliquots of all cultures were saved for virus titration and for Western blotting (see below). For comparative SILAC assays, equivalent numbers of L and H cells were mixed together, and the mixed cells were washed three times in >50 volumes of ice-cold phosphate-buffered saline (PBS). For assays to confirm differential infection status, infected and mock-infected cells were processed separately. In assays destined for SDS-PAGE separations, washed cells were swollen in hypotonic buffer (10 mM NaCl, 10 mM HEPES [pH 7.5], supplemented with 1.1 μM pepstatin A) for 30 min on ice, and then cells were lysed by 20 passages through a 30-gauge needle. Lysis was confirmed microscopically, and nuclei and insoluble membranes were pelleted at 5,000 × *g* for 10 min. The supernatant was saved as "cytosol." The nuclei and crude membranes were resuspended in 200 μl of 0.5% NP-40 and incubated on ice for 30 min, and nuclei were removed by pelleting at 5,000 × *g* for 10 min. The "crude membranes" (supernatant) were transferred to a fresh microcentrifuge tube, and electrophoresis sample buffer was added to each of the three fractions (nuclear pellet, crude membranes, and cytosol), which were then frozen at −80°C until further processing took place. In assays destined for liquid chromatographic separations, washed cells were lysed with 0.5% NP-40, supplemented with 1.1 μM pepstatin A, and incubated on ice for 30 min, and nuclei were removed by pelleting at 5,000 × *g* for 10 min. The cytosol and soluble membranes (supernatant) were transferred to fresh microcentrifuge tubes, and the two fractions (nuclear pellet and supernatant) were frozen at −80°C until further processing took place.

Immunoblotting. Aliquots of unlabeled and L- and H-labeled infected and mock-infected cells were separately harvested and dissolved with 0.5% NP-40 as described above, and cytosolic fractions were collected, mixed with SDS electrophoresis sample buffer, heated to 95°C for 5 min, and resolved in a 5 to 15% minigradient SDS-PAGE gel (6.0 by 10.0 by 0.1 cm) at 180 V for 50 min (until the bromophenol blue tracking dye was at the gel bottom), and proteins were transferred to polyvinylidene difluoride (PVDF). The PVDF membranes were briefly stained with Ponceau to confirm protein transfer, blocked with 5% skim milk, and probed with various antibodies. Primary antibodies were mouse anti-influenza NP protein (74), α-GAPDH, α-vimentin, α-β-2-microglobulin, alpha vasodilatory-stimulated phosphoprotein (α-VASP), rabbit anti-actin, α-Rock2, α-Akt, α-cytokeratin 10, α-Bid, and goat anti-poly(ADP-ribose) polymerase (PARP). Secondary antibodies were Alexa488-conjugated goat anti-mouse for NP and GAPDH, Alexa488-conjugated goat anti-rabbit for actin, or the appropriate horseradish peroxidase (HRP)-conjugated rabbit anti-mouse, goat anti-rabbit, or rabbit anti-goat for all other proteins. HRP was detected by enhanced chemiluminescence, film and fluorescent secondary antibodies were visualized, and band intensities were measured with an Alpha Innotech FluorChemQ MultiImage III instrument.

Protein digestion. Protein content in the cytosolic and soluble membrane fractions collected as described above was determined using a bicinchoninic acid (BCA) protein assay kit (Pierce; Rockford, IL) and bovine serum albumin standards. After protein concentration determinations, samples were diluted with freshly made 100 mM ammonium bicarbonate to provide concentrations of ~1 mg/ml and a pH of ~8. Three hundred microliters of each sample (~300 μg of protein) was reduced, alkylated, and trypsin digested using the following procedure. Thirty microliters of freshly prepared 100 mM dithiothreitol (DTT) in 100 mM ammonium bicarbonate was added. The samples were then incubated for 45 min at 60°C. Thirty microliters of freshly prepared iodoacetic acid (500 mM solution in 100 mM ammonium bicarbonate) was added to each tube, and the tubes were then incubated for 30 min at room temperature in the dark. Finally, 50 μl of 100 mM DTT solution was added to quench the excess iodoacetic acid. Samples were digested overnight at 37°C with 6 μg of sequencing grade trypsin (Promega, Madison, WI). The samples were lyophilized and stored at −80°C.

Peptide fractionation using 2-D RP HPLC. A newly developed orthogonal procedure (32, 67) was employed for 2-D reversed-phase (RP) high-pH/RP low-pH peptide fractionation. Lyophilized tryptic digests were dissolved in 200 μl of 20 mM ammonium formate (pH 10) (buffer A for first-dimension separation), injected onto a 1- by 100-mm XTerra (Waters, Milford, MA) column, and fractionated using a 0.67% acetonitrile-per-minute linear gradient (Agilent 1100 Series high-performance liquid chromatography [HPLC] system; Agilent Technologies, Wilmington, DE) at a 150-μl/min flow rate. Sixty 1-min fractions were collected (covering an ~40% acetonitrile concentration range) and concatenated using procedures described elsewhere (22, 67); the last 30 fractions were com-

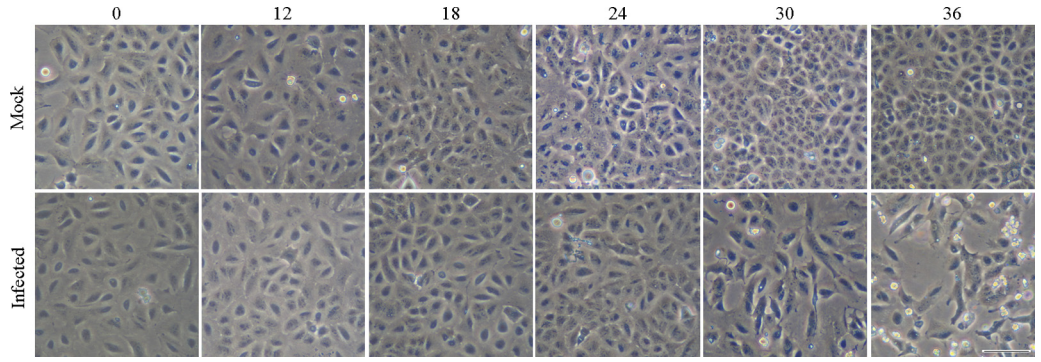

FIG. 1. Photomicrographs of A549 cells infected with A/PR/8/34 at an MOI of 7 PFU/cell (bottom) or mock-infected (top) for the indicated hours postinfection (indicated at the top). Scale bar, 100 μm.

bined with the first 30 fractions in sequential order (i.e., 1 with 31; 2 with 32, etc.). Combined fractions were vacuum dried and redissolved in buffer A for the second-dimension RP separation (0.1% formic acid in water).

A splitless nano-flow Tempo LC system (Eksigent, Dublin, CA) with 20 μl sample injection via a 300-μm by 5-mm PepMap100 precolumn (Dionex, Sunnyvale, CA) and a 100-μm by 200-mm analytical column packed with 5 μm Luna C18(2) (Phenomenex, Torrance, CA) were used in the second-dimension separation prior to mass spectrometry (MS) analysis. Both eluents A (water) and B (acetonitrile) contained 0.1% formic acid as an ion-pairing modifier. A 0.33% acetonitrile-per-minute linear gradient (0 to 30% B) was used for peptide elution, providing a total 2-h run time per fraction in the second dimension.

Mass spectrometry, bioinformatics, and data mining. A QStar Elite mass spectrometer (Applied Biosystems, Foster City, CA) was used in a data-dependent tandem MS (MS/MS) acquisition mode. One-second-survey MS spectra were collected (m/z 400 to 1,500), followed by MS/MS measurements on the three most intense parent ions (80 counts/s threshold, +2 to +4 charge state, m/z 100 to 1,500 mass range for MS/MS), using the manufacturer's "smart exit" (spectral quality 5) settings. Previously targeted parent ions were excluded from repetitive MS/MS acquisition for 60 s (50-mDa mass tolerance). Protein Pilot 2.0 (Applied Biosystems) software was used for protein identification and quantitation. Raw data files (30 in total for each run) were submitted for simultaneous searches using standard SILAC settings for QStar instruments. Proteins for which at least two fully trypsin-digested L and H peptides were detected at >99% confidence were used for subsequent comparative quantitative analysis.

Raw MS data files were analyzed by Protein Pilot, version 2.0, using the nonredundant human gene database. Proteins, and their confidences and L/H ratios, were returned with GeneInfo Identifier (gi) accession numbers.

Differential regulation within each experimental data set was determined by normalization of each data set, essentially as described previously (43). Briefly, every L/H ratio was converted into $\log_2$ space to determine geometric means and facilitate normalization. The average $\log_2$ L/H ratios and standard deviation of the $\log_2$ L/H ratios were determined for each data set, both before and after computational removal of the few (up to 12) significant outliers found in a few data sets. Every protein's $\log_2$ L/H ratio was then converted into a z-score, using the formula:

$$\text{z-score } (\sigma) \text{ of [b]} = \frac{\text{Log}_2 \text{ L/H[b]} - \text{Average of } (\log_2 \text{ of each member, a } \ldots. \text{ n})}{\text{Standard deviation of } (\log_2 \text{ of each member, a } \ldots. \text{ n})}$$

where b represents an individual protein in a data set population (a….n), and the z-score is the measure of how many standard deviation units (expressed as "σ") that protein's $\log_2$ L/H ratio is away from its population mean. Thus, a protein with a z-score of >1.645σ indicates that that protein's differential expression lies outside the 90% confidence level, >1.960σ indicates that it is outside the 95% confidence level, 2.576σ indicates 99% confidence, and 3.291σ indicates 99.9% confidence. Z-scores of >1.960 were considered significant. GeneInfo Identifier numbers of all significantly regulated proteins were converted into HUGO nomenclature committee (HGNC) identifiers (IDs) by Uniprot (http://www.uniprot.org/), HGNC terms were submitted to and analyzed by the DAVID bioinformatic suite at the NIAID, version 6.7 (19, 41), and gene ontologies were

TABLE 1. Number of proteins, $\log_2$ L/H ratio means and standard deviations, and z-scores of SILAC-labeled proteins identified by various purification schemes

Purification method	No. of proteins	Mean $\log_2$ L/H ratio	SD $\log_2$	Z-scores[a]		
				±1.960σ (95%)	±2.576σ (99%)	±3.291σ (99.9%)
SDS-PAGE/LC						
1 Cytosol	248	0.029	0.565	8, 6	8, 4	8, 1
Crude membranes	273	0.085	0.531	9, 5	8, 3	8, 2
Nuclear	262	0.083	0.678	15, 1	14, 0	11, 0
2 Cytosol	467	−0.034	0.478	20, 9	9, 6	4, 4
Crude membranes	524	0.011	0.422	22, 10	14, 8	11, 2
Nuclear	478	0.003	0.415	18, 12	13, 3	10, 2
2-D HPLC						
1	1,890	0.013	0.633	44, 52	25, 35	20, 23
2	846	0.046	0.506	22, 15	17, 9	14, 5
3 technical (1)	2,509	−0.030	0.539	47, 67	33, 42	23, 30
3 technical (2)	2,574	−0.020	0.533	55, 65	35, 37	26, 29
Combined	3,173	−0.025	0.537			

[a] The first value is the number of upregulated proteins outside the indicated confidence level; the second number is the number of downregulated proteins outside the indicated confidence level.

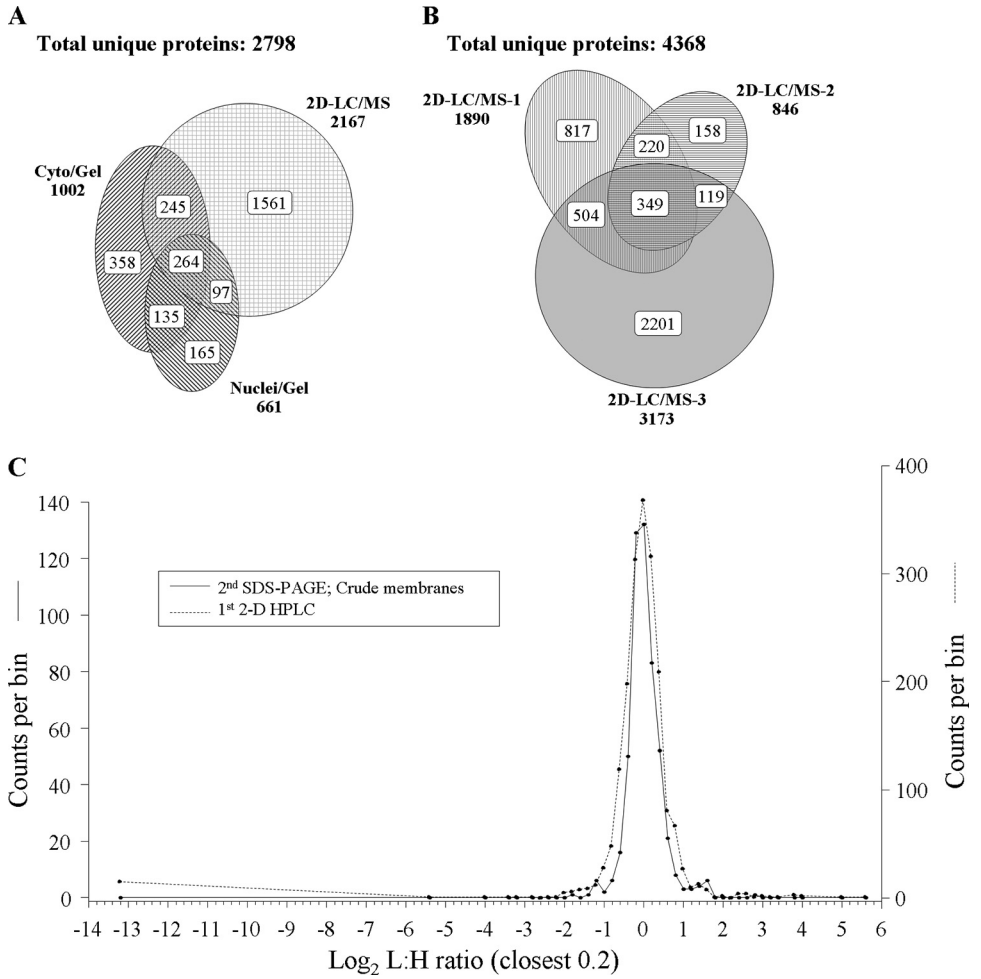

FIG. 2. Distributions of proteins identified in various experiments. (A and B) Venn diagrams of the numbers of identified proteins from various analyses. (A) Proteins from A/PR/9/34-infected A549 cells were fractionated into the cytosolic plus crude membrane (Cyto/Gel) and nuclei (Nuclei/Gel) fractions, resolved in SDS-PAGE, and then subjected to tryptic digest before 1-D LC/MS. Alternatively, proteins were harvested from cytosolic and crude membrane fractions and digested with trypsin, and then peptides were resolved by 2-D orthogonal LC/MS (2-D LC/MS). Results were compiled from two replicate experiments. (B) Proteins identified by the three separate 2-D LC/MS analyses. Proteins from the two technical replicate analyses of the third 2-D LC/MS run were merged prior to being combined with other data. (C) Frequency distributions of identified proteins in two influenza virus-infected A549 sample sets, with L/H ratios expressed as $\log_2$ values. Positive values represent upregulated host proteins in virus-infected cells; negative values represent downregulated host proteins. Only the distributions of one SDS-PAGE analysis and one 2-D LC/MS analysis are shown for clarity. Note that distributions are not identical, with different peak breadths, and not perfectly normal, with the 2-D LC/MS sample exhibiting several substantially downregulated proteins at approximately $-13\log_2$. Characteristics of all SDS-PAGE and 2-D LC/MS protein distributions, mean $\log_2$ L/H ratios, and standard deviations of $\log_2$ L/H ratios are shown in Table 1.

examined with the "FAT" data sets. The gi numbers were also submitted to, and pathways constructed with, Ingenuity Pathway Analysis (IPA) software.

RESULTS

Kinetics of influenza virus-induced cytopathology in cultured A549 cells. One of the key parameters for determining virus-induced alterations, and in separating such alterations from general stress responses related to cell death late in infection, is to determine when cytopathic effects (CPE) are manifested in the model system. Accordingly, we initially infected our A549-cultured human lung cells with influenza strain A/PR/8/34 (H1N1; PR8) at multiplicities of 7 PFU per cell (>99% of cells are initially infected as predicted by the Poisson distribution), and they were microscopically monitored for cell viability and CPE over time. Cells infected with PR8 and cultured for 24 h or less demonstrated no detectable CPE; there was minimal CPE detectable at 30 h postinfection (hpi), and CPE was readily apparent at later time points (Fig. 1). Therefore, in subsequent experiments, A549 cells were infected with the same MOI of PR8, cultured for 24 h, and processed in order to allow the virus to exert maximal effects without demonstrable CPE.

Two-dimensional HPLC provides more extensive protein identification than 1-D SDS-PAGE/1-D LC/ESI-MS. Eukaryotic cells possess highly complex proteomes, and peptide sample complexity must be reduced prior to MS-based interrogation (reviewed in references 23 and 75). There are several strategies for reducing sample complexity. We initially evaluated and compared gel-based purification of intact cellular proteins to HPLC purification of digested peptides. Equiva-

TABLE 2. A549 proteins increased >95% confidence[a]

Accession no.	HGNC ID	Name/description	L/H ratio[c]	Biological replicate	Z-score				
					2-D HPLC/MS[b]				SDS-PAGE[d]
					A	B	2DLC1	2DLC2	
Proteins measured in >1 biologic replicate									
gi|4755085	COL1A1	Pro alpha 1(I) collagen	17.307	2					**5.845**
gi|6013427	ALBU	Serum albumin precursor	9.979	2			**6.104**		**3.948**
gi|5031841	KRT6B	Keratin 6B	8.514	3					**6.448**
gi|547749	K1C10	Keratin, type I cytoskeletal 10 (cytokeratin 10) (CK-10) (keratin 10) (K10)	7.214	7	**6.069**	**11.870**			**6.434**
gi|5030431	VIME	Vimentin	6.944	2			**3.664**	**6.347**	
gi|5031839	K2C6A	Keratin 6A	5.939	3	**4.559**				**3.044**
gi|55956899	K1C9	Keratin 9	5.700	7			**5.481**		**5.888**
gi|17318569	KRT1	Keratin 1	5.141	8	**8.213**	**12.290**	**2.308**		**5.600**
gi|49456703	Q6FH82	IFITM2	5.002	2					**6.397**
gi|2996631	Q75MY7	MX2	4.968	2			**4.771**		**3.406**
gi|56757580	K2C5	Keratin, type II cytoskeletal 5 (cytokeratin 5 [CK-5]) (keratin 5 [K5]) (58-kDa cytokeratin)	4.273	2					**4.445**
gi|47132620	K22E	Keratin 2	4.243	7		**5.140**			**5.913**
gi|15431310	K1C14	Keratin 14	3.762	4					**8.348**
gi|48146249	B2 M	Beta-2-microglobulin	2.788	2					**3.775**
gi|14550514	UCRP	ISG15 ubiquitin-like modifier	2.735	3					**6.499**
gi|4580013	SNX6	Sorting nexin-6, TRAF4-associated factor 2	2.608	2	−0.557			**6.024**	
gi|55960992	H2A2C	Histone 2, H2ac	2.495	2				**4.848**	0.098
gi|55961043	SF13A	FUS-interacting protein (serine-arginine rich) 1	2.293	2			**2.575**		1.807
gi|13279173	CSN4	COP9 constitutive photomorphogenic homolog subunit 4 (arabidopsis)	2.287	2	0.040			**4.640**	
gi|34784772	GPI	Glucose-6-phosphate isomerase	2.118	3			**6.172**		−0.602
gi|34783347	RAB15	RAB15, member RAS oncogene family	1.959	3		**5.252**			0.148
gi|56122599	Q5Q9Z3	Leukemia multidrug resistance-associated protein	1.865	2					**2.225**
gi|7705893	DCTN4	Dynactin 4 (p62)	1.864	2	**2.884**	**4.081**	−0.086		
gi|4218955	FLNC	Gamma-filamin	1.847	2		−0.325		**3.784**	
gi|13623669	HEXI1	Hexamethylene bis-acetamide inducible 1	1.746	2	**2.313**	**2.035**		0.833	
gi|39645500	SCYL2	SCY1-like 2 (*Saccharomyces cerevisiae*)	1.699	2		**2.414**	0.396		
gi|40850903	Q549N5	Signal recognition particle receptor, B subunit	1.613	2	**2.626**	**2.207**	0.151		
gi|49457320	Q6FGE5	S100A10	1.567	6				0.324	**2.112**
gi|6031192	MPCP	Solute carrier family 25 member 3 isoform a precursor	1.538	3			**3.114**		−0.092
gi|3088341	RS21	Ribosomal protein S21	1.481	2					**2.799**
gi|29839750	AT1A3	Sodium/potassium-transporting ATPase alpha-3 chain (sodium pump 3) (Na^+/K^+ ATPase 3) [alpha(III)]	1.386	2			**2.114**		−0.994
gi|57160805	SH3L1	SH3 domain binding glutamic acid-rich protein-like	1.368	2		−0.316			**2.355**
gi|37514845	NUDC1	NudC domain containing 1	1.349	2	**2.130**		−0.422		0.000
gi|55661047	RRBP1	Ribosome binding protein 1 homolog, 180 kDa (dog)	1.323	2				−0.240	**2.066**
gi|57162423	5NTD	5′ nucleotidase, ecto (CD73)	1.271	4	**4.652**	**2.585**			1.392
gi|984325	6PGD	Phosphogluconate dehydrogenase	1.148	3					**2.775**
Proteins measured in only 1 biologic replicate but in 2 technical replicates									
gi|435476	K1C9	Cytokeratin 9	33.818		**10.613**	**8.434**			
gi|57864582	HORN	Hornerin	17.710		**7.367**	**8.212**			
gi|435675	MT1X	MT-1l protein	4.544		**4.275**	**3.971**			
gi|345829	*[e]	Ubiquitin carrier protein E2, human	3.684		**4.948**	**2.154**			
gi|5902146	UBE2C	Ubiquitin-conjugating enzyme E2C isoform 1	3.438		**2.942**	**3.808**			
gi|57208424	CRNL1	Crn, crooked neck-like 1 (*Drosophila*)	3.131		0.861	**5.404**			
gi|52352803	ZNT1	Solute carrier family 30 (zinc transporter), member 1	2.644		**2.504**	**2.827**			
gi|5817162	DREB	Hypothetical protein	2.577		1.882	**3.317**			

gi|36327	METK2	*S*-adenosylmethionine synthetase	2.355	**2.697**	**2.007**			
gi|4507711	TTC1	Tetratricopeptide repeat domain 1	2.316	1.692	**2.932**			
gi|4529892	HSP71	HSP70-2	1.949	1.590	**2.101**			
gi|4689140	GBRL2	Ganglioside expression factor 2 homolog	1.932	**2.350**	1.285			
gi|56207188	SSU72	Novel protein (HSPC182)	1.759	**2.213**	0.915			
gi|20986531	MK01	Mitogen-activated protein kinase 1	1.738	1.011	**2.064**			
gi|21619574	OSGEP	*O*-sialoglycoprotein endopeptidase	1.711	**1.971**	1.011			
gi|54696790	PRAF1	Rab acceptor 1 (prenylated)	1.644	**2.075**	0.688			
Proteins measured only once								
gi|13650074	HBA	Hemoglobin alpha-1 globin chain	121.222		**13.028**			
gi|18418633	HBB	Mutant beta-globin	47.517			**8.781**		
gi|38788274	BPTF	Fetal Alzheimer antigen isoform 1	30.503			**7.770**		
gi|4885215	ERBB4	v-erb-a erythroblastic leukemia viral oncogene homolog 4 isoform JM-a/CVT-1 precursor	25.424	**8.724**				
gi|181402	K22E	Epidermal cytokeratin 2	18.987	**7.942**				
gi|55958235	MARH5	RING finger protein 153	16.959		**7.702**			
gi|10440389	Q9H7N8	FLJ00030 protein	16.475			**6.366**		
gi|31815	DHE4	Glutamate dehydrogenase [NAD(P)$^+$]	15.471		**7.454**			
gi|19923667	RSAD2	Radical *S*-adenosyl methionine domain containing 2	14.315			**6.046**		
gi|34416	TRFL	Precursor (amino acids 19 to 692)	14.032			**6.000**		
gi|13623477	WDR4	WD repeat domain 4	13.968		**7.177**			
gi|2183299	AL1A1	Aldehyde dehydrogenase 1	12.845		**6.950**			
gi|4557701	K1C17	Keratin 17	12.223					**6.641**
gi|34190642	TRXR3	TXNRD3 protein	12.096		**6.787**			
gi|38541654	Q53YJ2	Dermcidin	9.891		**6.242**			
gi|7688699	Q9P0H9	RER1 protein	9.749	**6.156**				
gi|51470993	*	Predicted: similar to sucb isoform 1	9.129	**5.980**				
gi|51467148	*	Predicted: similar to tropomyosin 4	9.005		**5.988**			
gi|4557325	APOE	Apolipoprotein E precursor	8.927			**4.969**		
gi|9437341	Q9NRV0	x 004 protein	7.502			**4.573**		
gi|1911770	NCOR2	T3 receptor-associating cofactor 1; TRAC-1	7.469	**5.442**				
gi|609308	TCPG	Cytoplasmic chaperonin hTRiC5	7.181	**5.337**				
gi|27734452	RAB15	Ras-related protein Rab-15	6.862		**5.252**			
gi|4186185	VIPAR	Unknown	6.835			**4.361**		
gi|3075509	PLK2	Serum-inducible kinase	6.041			**4.080**		
gi|22671717	HBA	Hemoglobin alpha-2	5.865			**4.012**		
gi|541678	D3DTU3	hbZ17	5.798			**3.986**		
gi|57162615	ANK3	Ankyrin 3, node of Ranvier (ankyrin G)	5.631			**3.919**		
gi|17390794	TISB	Zinc finger protein 36, C3H type-like 1	5.303			**3.783**		
gi|40788366	TM63A	KIAA0792 protein	4.782				**4.367**	
gi|115143	BTF3	Transcription factor BTF3 (RNA polymerase B transcription factor 3)	4.745		**4.253**			
gi|3763907	RBP56	RBP56/hTAFII68	4.704					**4.006**
gi|49065664	KATNAL2	Katanin p60 subunit A-like 2	4.627	**4.160**				
gi|56204086	D3DVZ4	C20orf16	4.450	**4.055**				
gi|28559080	SMOX	Polyamine oxidase isoform 4	3.868		**3.700**			
gi|55666285	LCN1L1	Lipocalin 1-like 1	3.808					**3.473**
gi|14043853	KITH	Thymidine kinase 1, soluble	3.803			**3.024**		
gi|55664988	KHDR1	KH domain containing, RNA binding, signal transduction associated 1	3.641				**3.591**	
gi|51477696	PARVB	Parvin, beta isoform a	3.628	**3.508**				
gi|14602868	GLTP	Glycolipid transfer protein	3.597	**3.485**				
gi|56417844	ARK73	Aldo-keto reductase family 7, member A3 (aflatoxin aldehyde reductase)	3.546			**2.865**		
gi|11036646	H2BFS	H2B histone family, member S	3.521				**3.495**	
gi|56404694	RIOK3	Serine/threonine-protein kinase RIO3 (RIO kinase 3) (sudD homolog)	3.133			**2.583**		
gi|40548422	CHM4A	Chromatin-modifying protein 4A	3.130					**3.516**
gi|386849	K2C6B	Keratin type II	3.115		**3.113**			
gi|39843342	A16L1	APG16L beta	3.090			**2.551**		
gi|27657357	Q861B7	MHC class I antigen	2.933	**2.939**				

Continued on following page

TABLE 2—*Continued*

Accession no.	HGNC ID	Name/description	L/H ratio[c]	Biological replicate	Z-score				
					2-D HPLC/MS[b]				SDS-PAGE[d]
					A	B	2DLC1	2DLC2	
gi|3559910	CMC1	Aralar1	2.916		**2.923**				
gi|37515270	MACD1	LRP16 protein	2.867				**2.381**		
gi|5815178	TX264	Unknown	2.855						**3.557**
gi|1143492	GRP78	BiP	2.846		**2.858**				
gi|453155	K1C9	Keratin 9	2.792						**3.482**
gi|13937792	Q6FG85	Eukaryotic translation initiation factor 1B	2.778				**2.309**		
gi|1296662	PLEC1	Plectin	2.721					**2.761**	
gi|50949925	Q6AI07	Hypothetical protein	2.685						**3.348**
gi|9931112	Q9GJF2	Human leukocyte antigen Cw	2.659			**2.685**			
gi|55665435	B4DEB1	H3 histone, family 3A	2.659				**2.209**		
gi|47682981	GRPE2	GrpE-like 2, mitochondrial (*Escherichia coli*)	2.619				**2.175**		
gi|6730096	PAI1	Chain D, plasminogen activator inhibitor 1	2.619		**2.635**				
gi|4758544	HNRNPC	Heterogeneous nuclear ribonucleoprotein C isoform b	2.587			**2.610**			
gi|24659879	PRDX2	Peroxiredoxin 2	2.562				**2.124**		
gi|7209305	MRP7	FLJ00002 protein	2.518				**2.085**		
gi|4826774	UCRP	Interferon, alpha-inducible protein (clone IFI-15K)	2.504		**2.515**				
gi|7020602	MTMRC	Unnamed protein product	2.495				**2.064**		
gi|2143260	P3C2A	Phosphoinositide 3-kinase	2.454		**2.461**				
gi|22760981	Q8NC04	Unnamed protein product	2.331			**2.329**			
gi|48145713	Q6IBK5	GTF2F1	2.267		**2.249**				
gi|55959755	RPL29	Ribosomal protein L29	2.261					**2.233**	
gi|33357878	DCK	Chain B, structure of human Dck complexed with gemcitabine and Adp-Mg	2.167			**2.131**			
gi|56205909	RAB4A	RAB4A, member of RAS oncogene family	2.166			**2.130**			
gi|4240137	PCF11	KIAA0824 protein	2.136			**2.093**			
gi|38516	CAV1	Caveolin	2.091					**2.010**	
gi|2924620	SPIT2	Hepatocyte growth factor activator inhibitor type 2	2.044						**2.415**
gi|642239	1C03	Class I histocompatibility antigen HLA-CW3	1.866						**2.104**
gi|825616	ACTB	Unnamed protein product	1.819						**2.017**

[a] Protein is included if at least half of the biologic z-score values are $\geq 1.960\sigma$ (indicated by bolding) and there are no major disagreements between technical replicates A and B.
[b] 2-D HPLC runs; A and B refer to 2 technical replicates of a third biologic sample; 2DLC1 and 2DLC2 refer to the first and second 2-D HPLC runs.
[c] L/H ratio refers to the geometric mean of all $\log_2$ L/H values for each given gi number, expressed as relative protein quantity in infected cultures.
[d] Z-scores from multiple SDS-PAGE fractions are collapsed into a single most significant value for clarity.
[e] *, unable to map; record obsolete or removed.

lent numbers of PR8-infected $^{12}C_6$-Lys, $^{12}C_6{}^{14}N_4$-Arg (SILAC light), and mock-infected $^{13}C_6$-Lys, $^{13}C_6{}^{15}N_4$-Arg (SILAC heavy) A549 cells were mixed together, and various purification methods were tested. Initially, mixtures of L- and H-labeled entire cells were dissolved in electrophoresis sample buffer and resolved in a single gel lane of a 5 to 15% SDS-PAGE minigel, the entire gel lane was cut into 24 slices, and each slice was processed by in-gel trypsin digestion. Peptides were extracted and processed as detailed more fully in Materials and Methods by liquid chromatography/electrospray ionization mass spectrometry (LC/ESI-MS); this resulted in the identification of about 300 pairs of proteins (data not shown).

We then fractionated mixed L-H cells as described in Materials and Methods to generate crude cytosolic, membrane, and nuclear fractions, each of which were separately resolved by 1-D SDS-PAGE/1-D LC/ESI-MS as described above. Approximately 250 to 550 L-H protein pairs were detected and measured in each fraction in each of 2 biologic replicates, using stringent protein identification criteria of 2 complete L and H tryptic peptides and an identification confidence of ≥99% (Table 1). There were some common proteins found in different fractions, such that compilation of both 1-D SDS-PAGE/1-D LC/ESI-MS analyses identified 1,002 pairs of proteins in the combined cytosolic and membrane fractions (Fig. 2A). As an alternate strategy, equivalent L-H cell mixtures were washed and lysed with 0.5% NP-40 to obtain cytosolic and membrane fractions, proteins were digested with trypsin, and peptides were processed for 2-D HPLC/ESI-MS as detailed in Materials and Methods. Analyses of two separate biological replicates processed this way identified more than 2,100 pairs of proteins. More than 500 of the identified protein pairs were common to both the 1-D SDS-PAGE/1-D LC/ESI-MS and the 2-D HPLC/ESI-MS methods, and many proteins were also detected in the nuclear fractions (Fig. 2A).

Having established that 2-D HPLC/ESI-MS identified more than twice as many protein pairs as 1-D SDS-PAGE/1-D LC/ESI-MS, we then performed two technical 2-D HPLC/ESI-MS analyses in an additional biological experiment. These technical replicates identified a total of 3,173 unique cytosolic proteins (Table 1), of which 2,044 were common to both replicates. Comparisons of each of these 2,044 common protein's $\log_2$ ratios showed a correlation of $r^2 = 0.660$ (data not shown), indicating that most of the commonly identified proteins had similar L/H ratios in each technical replicate. Ten of the 2,044 proteins did not behave similarly in both replicate runs such that they differed in significance or direction of regulation. One protein (MGC2477) was measured as significantly upregulated 18-fold in one technical replicate but downregulated almost 2-fold in the other run. Nine other proteins appeared to be significantly up- or downregulated in one run (defined as described above) but were slightly regulated in the opposite direction in the other replicate. These 10 proteins were included in subsequent statistical analyses, but because we could not confidently establish whether each was up- or downregulated, we did not include them in lists of up- and downregulated proteins or in subsequent gene ontology and pathway analyses.

Influenza virus infection induces significant up- and downregulation of numerous cellular proteins. Combination of all 2-D LC-identified proteins with all 1-D SDS-PAGE/1-D LC-identified proteins resulted in the identification and measurement of 4,817 total unique protein pairs. Inspection of each protein's $\log_2$ distribution indicated variability in each data set's mean $\log_2$ value and in each data set's $\log_2$ standard deviation (Fig. 2C; Table 1). Thus, every protein's L/H ratio was converted into a z-score as described in Materials and Methods to allow interexperiment comparisons.

Stratification of each protein's L/H ratio and its z-score from each experimental run indicated that numerous proteins were identified in each experiment that could be considered significantly regulated. For example, of the 248 proteins identified in the first SDS-PAGE/LC-prepared cytosol sample, 8 were upregulated at 95% confidence and each of these was also upregulated at 99.9% confidence (Table 1). Six proteins in the same data set were downregulated at 95% confidence, but only one of these proteins was also downregulated at 99.9% confidence. Inspection of protein L/H ratios and z-scores indicated that most proteins differentially regulated at >95% confidence had L/H ratios altered by >1.6-fold, and most proteins differentially regulated at >99% confidence had L/H ratios altered by >2.2-fold. However, a number of proteins with L/H ratios in the range of 0.667 to 1.500 also had significant z-scores. For example, a protein might have an L/H ratio of 1.2 but be considered significant if it was a member of a population with a negative mean $\log_2$ L/H and a small standard deviation (i.e., 2nd cytosol sample), whereas another protein might have an L/H ratio of 2.2 but be considered nonsignificant if it was a member of a population with a positive mean $\log_2$ L/H ratio and a larger standard deviation (i.e., first nuclear sample). Thus, although some studies have set L/H ratio significance levels ranging from as little as 1.4-fold (29) or less to as much as 3-fold (49), we elected to assign significance based upon z-scores, with a few exceptions. Of the 4,817 total identified proteins, only 128 were found exclusively in the nuclei fractions derived from the preliminary limited 1-D SDS-PAGE/1-D LC analyses; thus, we focused further analyses on the 4,689 cytosolic proteins, with the expectation that the nuclear proteins will be studied more extensively at a later date.

Using the above criteria, we identified and measured 127 proteins that were significantly upregulated (Table 2). A protein was usually included in this table if a minimum of one-half of its biologic replicate z-scores were $>1.960\sigma$. Proteins were not considered significantly regulated if there were significant differences in their z-scores from the 2 technical replicates of the 3rd 2-D HPLC analysis. Some of the significantly upregulated proteins included vimentin and Mx2, known to be upregulated by inflammation and/or influenza virus infection, and both upregulated about 5- to 7-fold. Although the significance of each protein's fold change was based upon z-score, we also included every protein's average fold level alteration, determined by averaging each protein's $\log_2$ L/H value from every observation (see Table ST-1 in the supplemental material). A total of 153 proteins were significantly downregulated using the same inclusion and exclusion criteria as above (Table 3). Many of these, including 38 proteins (such as ARHGAP5, cyclophilin-33A, and the *Vav* 3 oncogene), were significantly downregulated (z-score $< -4.0\sigma$) >100-fold.

Validation of SILAC ratios by Western blotting. To confirm some of the SILAC-determined protein ratios, we analyzed selected proteins in infected and mock-infected cells by immunoblotting. Although there are a limited number of appropri-

TABLE 3. A549 proteins decreased >95% confidence[a]

Accession no.	HGNC ID	Name/description	L/H ratio[c]	Biological replicate	Z-score				
					2-D HPLC/MS[b]				SDS-PAGE[d]
					A	B	2DLC1	2DLC2	
Proteins measured in >1 biologic replicate									
gi|27597059	DNJC9	DnaJ homolog, subfamily C, member 9	0.009	2	−0.155	−0.554	**−21.013**		
gi|50949588	LS14A	Hypothetical protein	0.009	2	−0.279			**−26.334**	
gi|13124770	VKOR1	Vitamin K epoxide reductase complex, subunit 1 isoform 1	0.009	2		**−24.902**			−0.409
gi|37181648	WDR82	WD40 protein	0.011	2	0.593	0.061	**−21.013**		
gi|5821389	8ODP	MTH1a-Met83 (p26), MTH1b-Met83 (p22), MTH1c-Met83 (p21), MTH1d-Met83 (p18)	0.012	2		**−24.902**			1.014
gi|55665273	B9EKV4	Aldehyde dehydrogenase 9 family, member A1	0.057	2			−0.371	**−15.994**	
gi|45827757	TACC2	Transforming, acidic coiled-coil-containing protein 2 isoform a	0.074	2	**−24.615**	−1.545	−0.726		
gi|5726629	SNX12	Sorting nexin 12	0.227	2	−0.712	−0.442	**−6.243**		
gi|38511857	GSLG1	Golgi apparatus protein 1	0.342	2	**−3.394**	**−4.634**			**−2.215**
gi|9910266	KIF15	Kinesin family member 15	0.344	2	−1.462	**−2.124**	**−3.330**		
gi|33563340	MYH14	Myosin, heavy polypeptide 14	0.358	2	**−3.286**		−1.859		
gi|20384898	CTNB1	Beta-catenin	0.374	3			**−5.387**	−1.942	0.164
gi|5138999	NDUS3	NADH-ubiquinone reductase	0.416	2	−1.260	**−2.098**	**−2.564**		
gi|47678533	GTPB1	GTPBP1	0.425	2	−1.776		**−2.361**		
gi|55962101	IF4G3	Eukaryotic translation initiation factor 4 gamma 3	0.443	2	**−2.085**	−1.532	**−2.157**		
gi|51479145	BIG1	Brefeldin A-inhibited guanine nucleotide-exchange protein 1	0.461	2		**−2.619**	−1.315		
gi|21961441	STRN4	Striatin, calmodulin binding protein 4	0.537	2	**−4.143**		0.721		
gi|763122	RAB35	Ray	0.572	2	−1.786	**−2.023**			−1.110
gi|7582292	Q9NZE6	BM-010	0.576	2	−0.332	−1.135			**−2.369**
gi|4886522	Q75MJ1	Hypothetical protein	0.584	2	**−3.130**		0.236		
gi|32698702	HECTD1	HECT domain containing 1	0.605	2	**−3.042**	−1.500	−0.345		
gi|21752190	Q8N9Z3	Unnamed protein product	0.606	2			0.654		**−4.459**
gi|4098297	IF2B3	Koc1	0.610	2	**−1.988**	−1.796			−0.947
gi|520587	KPCD	Protein kinase C delta-type	0.611	2			**−2.028**	−0.387	
gi|27881820	UN45A	Unc-45 homolog A (*Caenorhabditis elegans*)	0.638	2		0.073	**−2.099**		
gi|12803105	NUCB1	Nucleobindin 1	0.656	4	**−2.422**	**−2.116**	1.074	**−2.188**	−1.659
gi|28422560	NUP53	NUP35 protein	0.700	2	**−2.049**	−1.554			−0.096
gi|7022606	PPME1	Unnamed protein product	0.716	2			0.043	**−2.070**	
gi|4808278	ERG7	Lanosterol synthase	0.721	2	−0.973	**−2.703**	0.081		
gi|6563210	NSF1C	P47 protein	0.722	2					**−2.753**
gi|57014043	Q5I6Y6	Lamin A/C transcript variant 1	0.756	3	**−2.320**	**−2.094**			−0.199
gi|36155	RIR2	Small subunit ribonucleotide reductase	0.759	2	−1.575	**−2.115**	0.322		
gi|5726310	1433G	14-3-3 gamma protein	0.812	2					**−2.185**
gi|913174	LAP2A	TRPP	0.847	3			−0.325		**−2.416**
gi|54648253	FUBP2	KHSRP protein	0.950	6	−0.349	−0.068	0.893	−0.222	**−1.970**
Proteins measured in 1 biologic replicate only but in 2 technical replicates									
gi|5837964	Q564D3	Endothelial protein C receptor	0.0001	1	**−24.615**	**−24.902**			
gi|18490620	EPCR	Splicing factor, arginine/serine-rich 7, 35 kDa	0.0001	1	**−24.615**	**−24.902**			
gi|21361822	NDUFA13	NADH dehydrogenase (ubiquinone) 1 alpha subcomplex 13	0.0020	1	**−8.653**	**−24.902**			
gi|56550065	CPLX2	Complexin 2	0.0055	1	**−24.615**	**−3.229**			
gi|30354483	NAA40	*N*-acetyltransferase 11	0.0063	1	**−2.436**	**−24.902**			
gi|34530730	BTBDB	Unnamed protein product	0.0064	1	**−2.376**	**−24.902**			
gi|55960776	D3DVC8	Mitochondrial ribosomal protein L24	0.0065	1	**−2.290**	**−24.902**			
gi|4504009	AGAL	Galactosidase, alpha	0.0081	1	−1.051	**−24.902**			
gi|7657671	UBF1	Upstream binding transcription factor, RNA polymerase I	0.209	1	**−3.494**	**−4.840**			
gi|29791720	MET10	METT10D protein	0.223	1	**−3.919**	**−4.080**			

gi|39645799	Q6P3U7	RXRA protein	0.278	1	**−3.678**	**−3.131**			
gi|6730223	PROF2	Chain D, crystal structure of human profilin Ii	0.284	1	−0.987	**−5.718**			
gi|4503453	EDF1	Endothelial differentiation-related factor 1 isoform alpha	0.297	1	**−4.678**	−1.759			
gi|55960673	D3DPX7	Protein tyrosine phosphatase, receptor type F	0.313	1	**−3.252**	**−2.916**			
gi|25987321	Q54A15	URP1	0.324	1	**−2.317**	**−3.669**			
gi|55770850	CP24A	Cytochrome P450, family 24 precursor	0.364	1	**−2.915**	**−2.427**			
gi|23512254	SF01	SF1 protein	0.379	1	**−2.849**	**−2.284**			
gi|27769298	TRI25	Tripartite motif-containing 25	0.439	1	−1.915	**−2.425**			
gi|457262	Q7KZ24	Nuclease-sensitive element binding protein 1	0.449	1	**−2.011**	**−2.209**			
gi|10798851	FADS2	Fatty acid desaturase 2	0.472	1	**−2.412**	−1.539			
gi|10436660	Q9H7U7	Unnamed protein product	0.487	1	**−2.703**	−1.074			
gi|34999	CADH2	Unnamed protein product	0.487	1	**−2.253**	−1.522			
gi|4589628	PALLD	KIAA0992 protein	0.487	1	**−2.653**	−1.117			
gi|4503131	CTNNB1	Catenin (cadherin-associated protein), beta 1, 88 kDa	0.487	1	**−2.154**	−1.621			
gi|14124936	CO044	Chromosome 15, open reading frame 44	0.491	1	−1.782	**−1.960**			
gi|6492130	D3DU08	Urokinase receptor-associated protein uPARAP	0.491	1	−1.359	**−2.386**			
gi|2865163	TGFI1	Hic-5	0.499	1	**−2.376**	−1.271			
gi|4506409	RANBP3	RAN binding protein 3 isoform RANBP3-a	0.505	1	**−2.390**	−1.189			
gi|4759068	SCO1	Cytochrome oxidase-deficient homolog 1	0.507	1	−1.395	**−2.177**			
gi|27477134	PO210	Nucleoporin 210	0.509	1	**−2.405**	−1.135			
gi|7657683	XCT	Solute carrier family 7, (cationic amino acid transporter, y^+ system) member 11	0.542	1	**−2.229**	−0.972			
Proteins measured only once									
gi|49899808	RHG05	ARHGAP5 protein	0.0001	1			**−21.013**		
gi|47115211	ARL3	ARL3	0.0001	1				**−26.334**	
gi|5326759	KCC2B	Calcium/calmodulin-dependent protein kinase II beta e′ subunit	0.0001	1			**−21.013**		
gi|8571386	ICLN	Chloride ion current inducer protein I (Cln)	0.0001	1				**−26.334**	
gi|51594277	Q670S4	Hemoglobin Lepore-Baltimore	0.0001	1			**−21.013**		
gi|21739669	IWS1	Hypothetical protein	0.0001	1			**−21.013**		
gi|21739912	HTR7A	Hypothetical protein	0.0001	1			**−21.013**		
gi|34365494	CE044	Hypothetical protein	0.0001	1			**−21.013**		
gi|57997169	Q5JPD9	Hypothetical protein	0.0001	1			**−21.013**		
gi|57471655	KDM5C	Jumonji, AT-rich interactive domain 1C (RBP2-like)	0.0001	1			**−21.013**		
gi|6382020	RHG31	KIAA1204 protein	0.0001	1			**−21.013**		
gi|56081771	DUSTY	Receptor-interacting protein kinase 5	0.0001	1			**−21.013**		
gi|55960721	VAV3	vav 3 oncogene	0.0001	1			**−21.013**		
gi|23903	MK04	63-kDa protein kinase	0.0001	1		**−24.902**			
gi|29727	MYH7	Cardiac beta myosin-heavy chain	0.0001	1		**−24.902**			
gi|25990944	CLIC6	Chloride channel form B	0.0001	1	**−24.615**				
gi|2828149	PPIE	Cyclophilin-33A	0.0001	1		**−24.902**			
gi|115855	CBL	E3 ubiquitin-protein ligase CBL (signal transduction protein CBL) (proto-oncogene c-CBL) (casitas B-lineage lymphoma proto-oncogene) (RING finger protein 55)	0.0001	1		**−24.902**			
gi|6942004	EHD3	EH domain containing protein 2	0.0001	1	**−24.615**				
gi|18676696	MOV10	FLJ00247 protein	0.0001	1	**−24.615**				
gi|42407269	HELLS	Lymphoid specific helicase variant 8	0.0001	1		**−24.902**			
gi|20986521	MK08	Mitogen-activated protein kinase 8 isoform 4	0.0001	1		**−24.902**			
gi|3041706	MYH6	Myosin-heavy chain, cardiac muscle alpha isoform (MyHC-alpha)	0.0001	1		**−24.902**			
gi|55664366	STRBP	Spermatid perinuclear RNA binding protein	0.0001	1	**−24.615**				
gi|5454100	TACC1	Transforming, acidic coiled-coil-containing protein 1	0.0001	1		**−24.902**			
gi|35438	PGK2	Unnamed protein product	0.0001	1	**−24.615**				
gi|13124617	VTI1B	Vesicle transport through interaction with t-SNAREs homolog 1B (vesicle transport v-SNARE protein Vti1-like 1) (Vti1-rp1)	0.0001	1		**−24.902**			
gi|7020344	MIO	Unnamed protein product	0.022	1			**−8.672**		
gi|46250008	PP4R4	KIAA1622	0.108	1			**−5.090**		
gi|51859376	H33	H3 histone, family 3A	0.131	1					**−5.138**

Continued on following page

TABLE 3—*Continued*

Accession no.	HGNC ID	Name/description	L/H ratio[c]	Biological replicate	Z-score				
					2-D HPLC/MS[b]				SDS-PAGE[d]
					A	B	2DLC1	2DLC2	
gi|46249414	LTBP1	Latent transforming growth factor beta binding protein 1 isoform LTBP-1L	0.148	1			**−4.380**		
gi|576554	ANT3	Antithrombin III variant	0.187	1			**−3.841**		
gi|21264337	ARAP3	Centaurin, delta 3	0.228	1			**−3.391**		
gi|4557707	L1CAM	L1 cell adhesion molecule isoform 1 precursor	0.243	1			**−3.244**		
gi|55664563	KI67	Antigen identified by monoclonal antibody Ki-67	0.253	1	**−3.626**				
gi|39932736	MYO5B	Myosin-5B (Myosin Vb)	0.265	1			**−3.046**		
gi|31127073	RANB9	RANBP9 protein	0.266	1			**−3.038**		
gi|7023521	FBX3	Unnamed protein product	0.275	1			**−2.964**		
gi|40788219	NRCAM	KIAA0343	0.277	1		**−3.443**			
gi|190133	AT2B1	Plasma membrane $Ca2^{+}$ pumping ATPase	0.279	1		**−3.420**			
gi|16741274	Q53SZ8	Prolactin regulatory element binding	0.279	1			**−2.929**		
gi|3413793	NB5R3	NADH-cytochrome b5 reductase	0.281	1					**−3.759**
gi|51467774	RPS3AP5	Predicted: similar to ribosomal protein S3a isoform 1	0.289	1					**−3.121**
gi|6468766	LCAP	Oxytocinase/insulin-responsive aminopeptidase, variant 1	0.292	1			**−2.827**		
gi|22761383	CAB45	Unnamed protein product	0.304	1	**−3.132**				
gi|55859586	NU188	Nucleoporin, 188 kDa	0.304	1			**−2.732**		
gi|55664592	ARGAL	Novel protein	0.319	1			**−2.625**		
gi|10799803	RBSK	Ribokinase	0.321	1			**−2.608**		
gi|6983729	MYL9	MYL9	0.325	1		**−3.007**			
gi|21311254	STXB6	Amisyn	0.330	1			**−2.546**		
gi|5689473	NUDC3	KIAA1068 protein	0.337	1			**−2.497**		
gi|45501300	Q6NXG4	WDR13 protein	0.338	1			**−2.491**		
gi|23273305	D3DS37	Jub, ajuba homolog (Xenopus laevis)	0.338	1			**−2.490**		
gi|1685075	PTPRJ	Density-enhanced phosphatase-1	0.342	1	**−2.817**				
gi|22902182	RAVR1	RAVER1 protein	0.348	1			**−2.425**		
gi|57160661	MIPEP	Mitochondrial intermediate peptidase	0.355	1			**−2.380**		
gi|27764863	SLC25A6	Solute carrier family 25, member A6	0.355	1	**−2.716**				
gi|50949497	ALO17	Hypothetical protein	0.364	1		**−2.700**			
gi|15559717	AP2A1	AP2A1 protein	0.368	1				**−2.941**	
gi|115351	CO5A2	Collagen alpha-2(V) chain precursor	0.381	1			**−2.222**		
gi|55960069	CJ076	Novel protein	0.387	1			**−2.185**		
gi|21706672	CRIP2	Cysteine-rich protein 2	0.387	1		**−2.531**			
gi|31874098	NRCAM	Hypothetical protein	0.388	1	**−2.477**				
gi|45501252	PRAX	Periaxin	0.389	1				**−2.780**	
gi|20306890	PSA7L	Proteasome (prosome, macropain) subunit, alpha type, 8	0.392	1		**−2.500**			
gi|57162346	DIAPH3	Diaphanous homolog 3 (*Drosophila*)	0.392	1			**−2.154**		
gi|292870	UFO	Tyrosine kinase receptor	0.392	1		**−2.497**			
gi|53791223	FINC	Fibronectin 1	0.403	1			**−2.094**		
gi|55957730	D3DVE6	WD repeat domain 42A	0.404	1			**−2.084**		
gi|48429194	UFO	Tyrosine-protein kinase receptor UFO precursor (AXL oncogene)	0.407	1	**−2.351**				
gi|12804489	MELPH	Melanophilin	0.412	1	**−2.318**				
gi|178743	APEX1	Apurinic endonuclease	0.415	1		**−2.347**			
gi|56204680	Q5T8R3	Solute carrier family 16 (monocarboxylic acid transporters), member 1	0.418	1					**−3.006**
gi|15488917	PRKCSH	Protein kinase C substrate 80 K-H	0.420	1		**−2.311**			
gi|57209070	Q5JTE2	RP3-337H4.4	0.421	1			**−1.994**		
gi|34531906		Unnamed protein product	0.425	1		**−2.280**			
gi|48255937	CD44	CD44 antigen isoform 2 precursor	0.425	1					**−2.946**
gi|1575607	FUBP2	FUSE binding protein 2	0.431	1					**−2.901**
gi|6969149	MCM3	MCM3 minichromosome maintenance deficient 3 (*S. cerevisiae*)	0.436	1					**−2.069**

gi|39753961	IQGA3	IQ motif containing GTPase-activating protein 3	0.444	1	**−2.160**		
gi|18860900	PTPRJ	Protein tyrosine phosphatase, receptor type, J precursor	0.448	1	**−2.136**		
gi|56204524	ARPC5	Actin-related protein 2-3 complex, subunit 5, 16 kDa	0.449	1			**−2.764**
gi|55665466	D3DV57	Novel protein (FLJ21919)	0.451	1			**−1.985**
gi|55665798	UBP2L	Ubiquitin-associated protein 2-like	0.471	1	**−2.000**		
gi|50949942	S4A7	Hypothetical protein	0.477	1	**−1.966**		
gi|1184699	SYYC	Tyrosyl-tRNA synthetase	0.479	1			**−2.149**
gi|30268334	CD44	Hypothetical protein	0.479	1			**−2.148**

[a] Protein is included if at least half of the biologic z-score values are ≥1.960σ (indicated by bolding) and there are no major disagreements between technical replicates A and B.
[b] 2-D HPLC runs; A and B refer to 2 technical replicates of a 3rd biologic sample; 2DLC1 and 2DLC2 refer to the first and second 2-D HPLC runs.
[c] L/H ratio refers to the geometric mean of all $\log_2$ L/H values for each given gi number, expressed as relative protein quantity in infected cultures.
[d] Z-scores from multiple SDS-PAGE fractions are collapsed into a single most significant value for clarity.

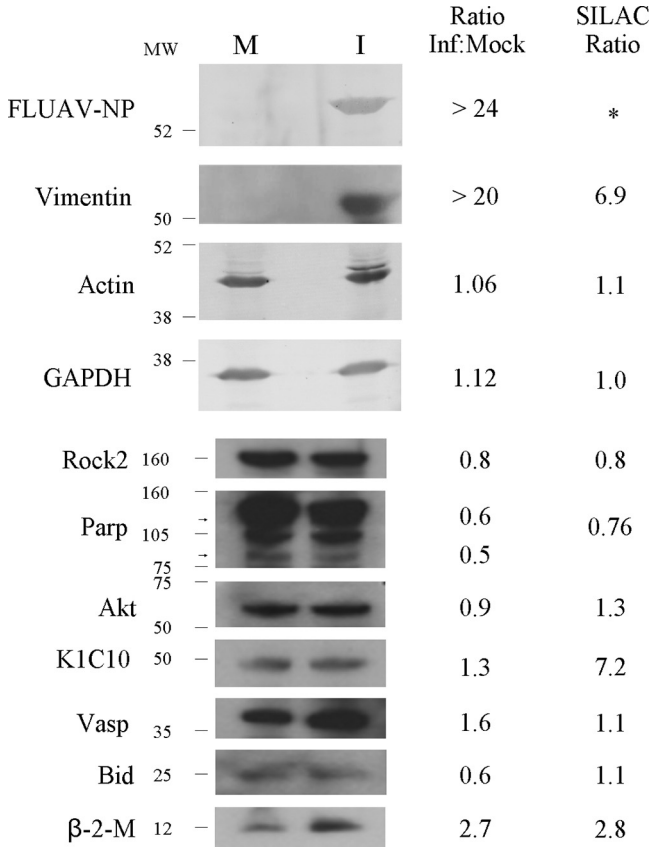

FIG. 3. Immunoblot analysis of host and influenza virus proteins in mock-infected (M) and influenza virus strain A/PR/8/34 (H1N1)-infected (I) A549 cells. Cells were harvested and lysed with 0.5% NP-40 detergent, nuclei were removed, and cytosolic fractions were dissolved in SDS electrophoresis sample buffer, resolved in s 5 to 15% minigradient SDS-PAGE, transferred to PVDF, and probed with various antibodies. Bands were visualized and intensities measured with an Alpha Innotech FluorChemQ MultiImage III instrument. Molecular weight standards are indicated at the left and ratios of each protein (infected divided by mock infected) are indicated for each protein at the right, along with SILAC-measured ratios (far right). *, no viral proteins were measured by SILAC because they were not present in mock-infected samples.

ate immunological reagents for most of the SILAC-measured proteins we identified in this study, we confirmed that vimentin and β-2-microglobulin were upregulated (Fig. 3). A number of proteins usually used as Western blot loading controls, such as GAPDH, which was found in every experiment at an L/H ratio of 1.1 ± 0.1 (mean ± standard deviation), and actin, with a measured average L/H ratio of 1.1, were present at equivalent levels in infected and mock-infected cells, as measured also by immunoblotting. Most other tested proteins were suggested by SILAC analysis to not be significantly regulated (L/H ratio of 1.0 ± 0.3 and z-scores within 0.5σ of 0.0), and these relative levels were generally confirmed by Western blotting. Of note, two major PARP bands in Fig. 3 have M_r values of 80 and 110 kDa, and immunoblots suggest that they are slightly downregulated 0.5- to 0.6-fold. PARP was returned as a number of gi identifications, including gi|337424 and gi|22902366, which had L/H ratios of about 0.76 and z-scores of approximately −0.2. We also tested the quantity of keratins, many of which appeared to be highly significantly upregulated in numerous SILAC exper-

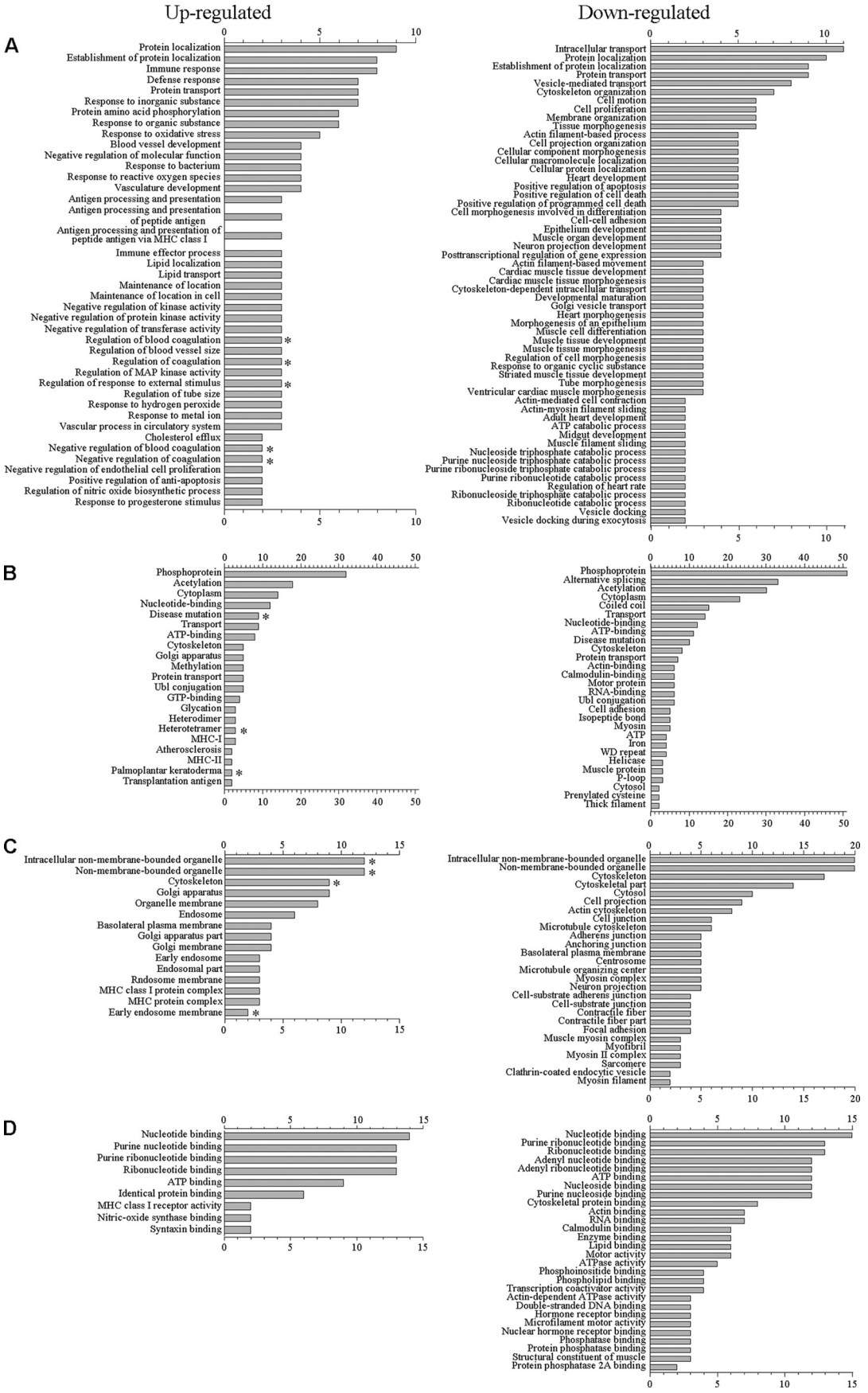
Up-regulated
Down-regulated
A
Protein localization
Establishment of protein localization
Immune response
Defense response
Protein transport
Response to inorganic substance
Protein amino acid phosphorylation
Response to organic substance
Response to oxidative stress
Blood vessel development
Negative regulation of molecular function
Response to bacterium
Response to reactive oxygen species
Vasculature development
Antigen processing and presentation
Antigen processing and presentation of peptide antigen
Antigen processing and presentation of peptide antigen via MHC class I
Immune effector process
Lipid localization
Lipid transport
Maintenance of location
Maintenance of location in cell
Negative regulation of kinase activity
Negative regulation of protein kinase activity
Negative regulation of transferase activity
Regulation of blood coagulation
Regulation of blood vessel size
Regulation of coagulation
Regulation of MAP kinase activity
Regulation of response to external stimulus
Regulation of tube size
Response to hydrogen peroxide
Response to metal ion
Vascular process in circulatory system
Cholesterol efflux
Negative regulation of blood coagulation
Negative regulation of coagulation
Negative regulation of endothelial cell proliferation
Positive regulation of anti-apoptosis
Regulation of nitric oxide biosynthetic process
Response to progesterone stimulus
Intracellular transport
Protein localization
Establishment of protein localization
Protein transport
Vesicle-mediated transport
Cytoskeleton organization
Cell motion
Cell proliferation
Membrane organization
Tissue morphogenesis
Actin filament-based process
Cell projection organization
Cellular component morphogenesis
Cellular macromolecule localization
Cellular protein localization
Heart development
Positive regulation of apoptosis
Positive regulation of cell death
Positive regulation of programmed cell death
Cell morphogenesis involved in differentiation
Cell-cell adhesion
Epithelium development
Muscle organ development
Neuron projection development
Posttranscriptional regulation of gene expression
Actin filament-based movement
Cardiac muscle tissue development
Cardiac muscle tissue morphogenesis
Cytoskeleton-dependent intracellular transport
Developmental maturation
Golgi vesicle transport
Heart morphogenesis
Morphogenesis of an epithelium
Muscle cell differentiation
Muscle tissue development
Muscle tissue morphogenesis
Regulation of cell morphogenesis
Response to organic cyclic substance
Striated muscle tissue development
Tube morphogenesis
Ventricular cardiac muscle morphogenesis
Actin-mediated cell contraction
Actin-myosin filament sliding
Adult heart development
ATP catabolic process
Midgut development
Muscle filament sliding
Nucleoside triphosphate catabolic process
Purine nucleoside triphosphate catabolic process
Purine ribonucleoside triphosphate catabolic process
Purine ribonucleotide catabolic process
Regulation of heart rate
Ribonucleoside triphosphate catabolic process
Ribonucleotide catabolic process
Vesicle docking
Vesicle docking during exocytosis
B
Phosphoprotein
Acetylation
Cytoplasm
Nucleotide-binding
Disease mutation
Transport
ATP-binding
Cytoskeleton
Golgi apparatus
Methylation
Protein transport
Ubl conjugation
GTP-binding
Glycation
Heterodimer
Heterotetramer
MHC-I
Atherosclerosis
MHC-II
Palmoplantar keratoderma
Transplantation antigen
Phosphoprotein
Alternative splicing
Acetylation
Cytoplasm
Coiled coil
Transport
Nucleotide-binding
ATP-binding
Disease mutation
Cytoskeleton
Protein transport
Actin-binding
Calmodulin-binding
Motor protein
RNA-binding
Ubl conjugation
Cell adhesion
Isopeptide bond
Myosin
ATP
Iron
WD repeat
Helicase
Muscle protein
P-loop
Cytosol
Prenylated cysteine
Thick filament
C
Intracellular non-membrane-bounded organelle
Non-membrane-bounded organelle
Cytoskeleton
Golgi apparatus
Organelle membrane
Endosome
Basolateral plasma membrane
Golgi apparatus part
Golgi membrane
Early endosome
Endosomal part
Rndosome membrane
MHC class I protein complex
MHC protein complex
Early endosome membrane
Intracellular non-membrane-bounded organelle
Non-membrane-bounded organelle
Cytoskeleton
Cytoskeletal part
Cytosol
Cell projection
Actin cytoskeleton
Cell junction
Microtubule cytoskeleton
Adherens junction
Anchoring junction
Basolateral plasma membrane
Centrosome
Microtubule organizing center
Myosin complex
Neuron projection
Cell-substrate adherens junction
Cell-substrate junction
Contractile fiber
Contractile fiber part
Focal adhesion
Muscle myosin complex
Myofibril
Myosin II complex
Sarcomere
Clathrin-coated endocytic vesicle
Myosin filament
D
Nucleotide binding
Purine nucleotide binding
Purine ribonucleotide binding
Ribonucleotide binding
ATP binding
Identical protein binding
MHC class I receptor activity
Nitric-oxide synthase binding
Syntaxin binding
Nucleotide binding
Purine ribonucleotide binding
Ribonucleotide binding
Adenyl nucleotide binding
Adenyl ribonucleotide binding
ATP binding
Nucleoside binding
Purine nucleoside binding
Cytoskeletal protein binding
Actin binding
RNA binding
Calmodulin binding
Enzyme binding
Lipid binding
Motor activity
ATPase activity
Phosphoinositide binding
Phospholipid binding
Transcription coactivator activity
Actin-dependent ATPase activity
Double-stranded DNA binding
Hormone receptor binding
Microfilament motor activity
Nuclear hormone receptor binding
Phosphatase binding
Protein phosphatase binding
Structural constituent of muscle
Protein phosphatase 2A binding

iments (L/H ratios of >5.0 and z-scores >3.0). However, immunoblotting indicated nearly equivalent amounts of cytokeratin 10 in infected and mock-infected cells. Thus, except for keratins, which are usually considered contaminants in MS experiments, immunoblotting validated the SILAC-determined values.

Proteins upregulated by influenza virus infection are associated with responses to stimuli and protein binding, localization, and transport, whereas downregulated proteins are associated with alternative splicing, nucleotide and nucleoside activities, catabolic and hydrolase functions, and cell adhesion.

Proteins, and their levels of regulation, were analyzed by a variety of means. Protein gi numbers were imported into Uniprot (http://www.uniprot.org/) and converted into HUGO nomenclature committee (HGNC) identifiers. Several hundred gi numbers could not be mapped to HGNC identifier numbers, and several hundred gi numbers were collapsed to about half as many genes. This resulted in about 3,900 unique HGNC IDs for the data set (see Table ST-1 in the supplemental material). Several of the different gi numbers that were collapsed into fewer genes may represent different isoforms of the same genes. The HGNC IDs that represented various sets of significantly upregulated and downregulated proteins at different confidence intervals of 95, 99, and 99.9% were then separately imported into DAVID (19, 41), gene identifications were converted to Entrez gene IDs by that suite of programs, and ontological functions were determined by GOTERM, PANTHER, and KEGG. We also analyzed the upregulated proteins at each confidence interval after removing keratins from the data sets. Biological processes, functional annotations, molecular functions, and cellular components identified at 95% confidence are depicted in Fig. 4, and data at all confidence levels are shown in Table ST-2 in the supplemental material.

Upregulated proteins were assigned to 41 GOTERM biological processes at 95% confidence (Fig. 4A, left; see also Table ST-2 in the supplemental material) that included immune and defense responses, responses to stress and to virus, MHC-I-mediated immunity pathways, and protein localization and transport. These upregulated proteins were also assigned to 21 functional groups (Fig. 4B) (including acetylation, cytoplasm, MHC-I and -II, phosphoprotein, and nucleotide binding), 19 cell component groups (Fig. 4C) (including cytoplasm, Golgi, and organelle membranes), and 9 molecular functions (Fig. 4D) (most notably nucleotide and ribonucleotide binding). PANTHER also assigned upregulated proteins to mRNA transcription regulation, cell structure, molecular binding, and MHC-I mediated immunity pathways (data not shown). Rerunning the analysis after removing keratins led to the removal of blood coagulation and cytoskeletal groups from the above categories. Downregulated proteins were assigned to 56 biological processes at 95% confidence (Fig. 4A, right; see also Table ST-2 in the supplemental material) that included localization determinants, transport, and positive regulation of apoptosis. These downregulated proteins were also assigned to 28 functional groups, including acetylation, phosphoproteins, and alternative splicing (Fig. 4B), 27 cell component groups (Fig. 4C) (including nonmembrane-bounded organelles and adhesion-related components), and 28 molecular functions (Fig. 4D) (including molecular binding and ATPase activity). PANTHER also assigned downregulated proteins to MHC-II-mediated immunity, nucleoside, nucleotide, and nucleic acid metabolism, adhesion, and cytoskeleton regulation. KEGG assigned proteins that had been downregulated >100-fold to a number of cell pathways, including focal adhesion, cell adhesion, and regulators of the actin cytoskeleton.

Protein gi numbers and levels of regulation were also imported into the Ingenuity Pathways Analysis (IPA) tool, and interacting pathways were constructed. A total of 18 pathways were identified at a confidence level of 95% or greater. Four of these pathways, each with 12 or more "focus" members (significantly up- or downregulated proteins), shared common members (Fig. 5A), and it was possible to build a single, merged pathway (Fig. 5B). The other 14 pathways consisted of several proteins but contained only a single focus protein (data not shown). The 4 networks that contained 12 or more focus members corresponded to hair, skin, and organ development, cell cycle, cell death, cancer, infection mechanisms, and antigen presentation pathways (Fig. 5C to F). Proteins present in the pathways and identified in our analyses as upregulated are depicted in shades of red and include Mx1, LTF, and VIM; proteins present in the pathways and identified as downregulated are shown in green and include ERC1, L1CAM, and CTNNB1; proteins present in the pathways and identified in our analyses but neither up- nor downregulated are depicted in gray and include SMAD3, SCARB1, and RNA Pol II; and proteins known to participate in the pathways but not identified in our analyses are shown in white and include MYC, MAP3K1, and TP53. IPA analyses identify interaction nodes. For example, several of the highly upregulated proteins interact with a few other proteins, but some, such as VIM and KHDRBS1, interact with four or more. Similarly, a few of the downregulated proteins interact with few partners, but several, including CTNNB1, appear as interaction "hubs." We identified numerous other interaction hubs, such as SCARB1, CHUK, HSPB1, SMAD3, CTNND1, TIAL1, and SMAD2, which were not themselves significantly altered but which interacted with several differentially regulated proteins.

DISCUSSION

A number of studies have defined the cellular networks that are required or manipulated by influenza infection by use of

FIG. 4. Gene ontology analyses of upregulated and downregulated proteins. The proteins identified in Tables 2 and 3, as well as nonkeratin proteins in Table 2, were imported into the DAVID gene ontology suite of programs at the NIAID, gene identifications were converted by that program, and ontological functions were determined by GOTERM. (A) Biological processes; (B) functional annotations; (C), cellular components; and (D) molecular functions. The numbers of identified genes associated with each group, identified at a confidence level of 95% are illustrated. *, processes, functions, and cellular components that are removed when keratins are excluded from the input gene list. Additional lists of functional groups, processes, and components at different confidence limits are indicated in Table ST-2 in the supplemental material.

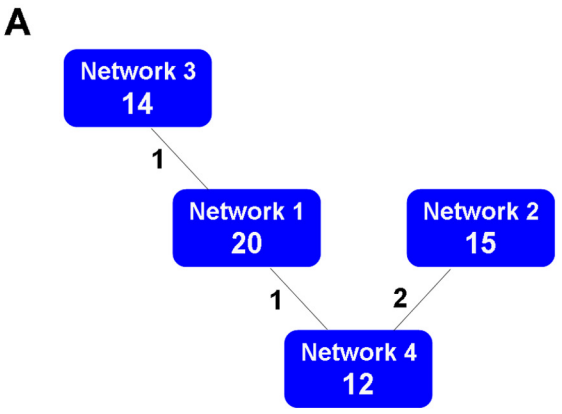

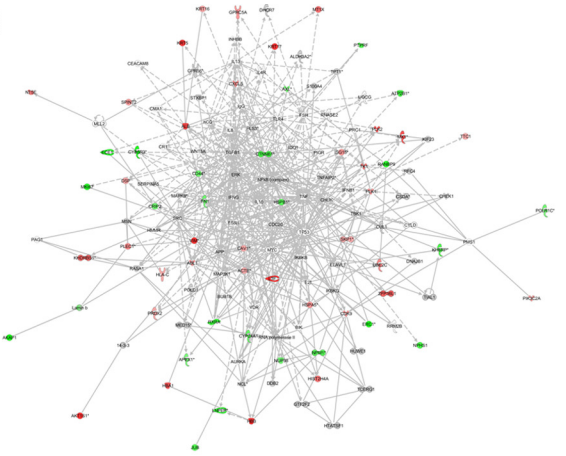

C Network 1: Hair & skin development and function, Organ development, Cancer

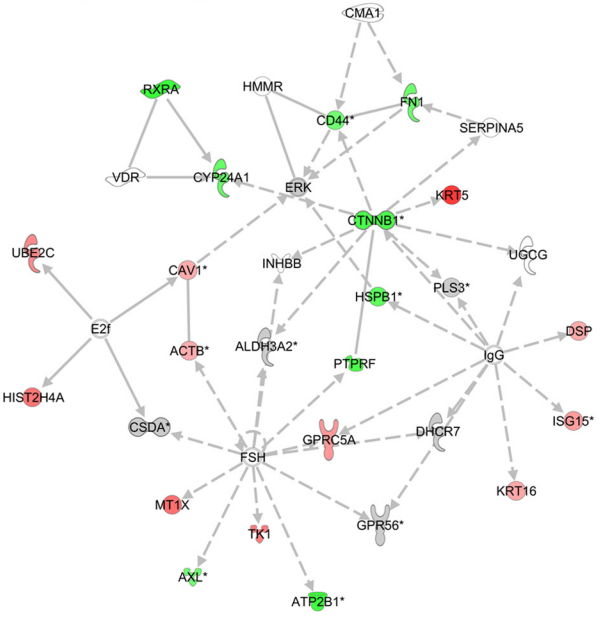

D Network 2: Infection mechanism, Cell-mediated immune response, Hematopoiesis

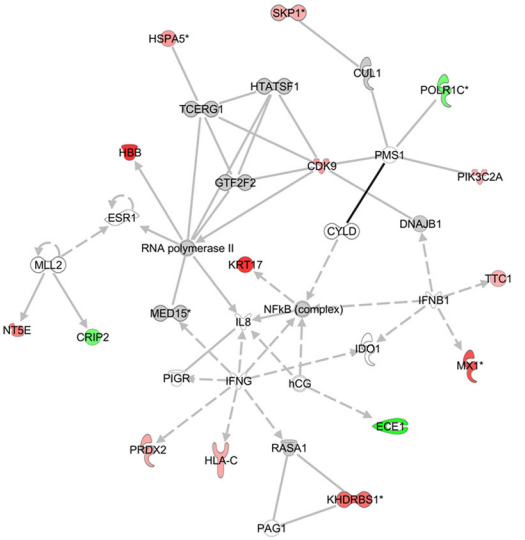

E Network 3: Cell cycle, Cancer, Cell death

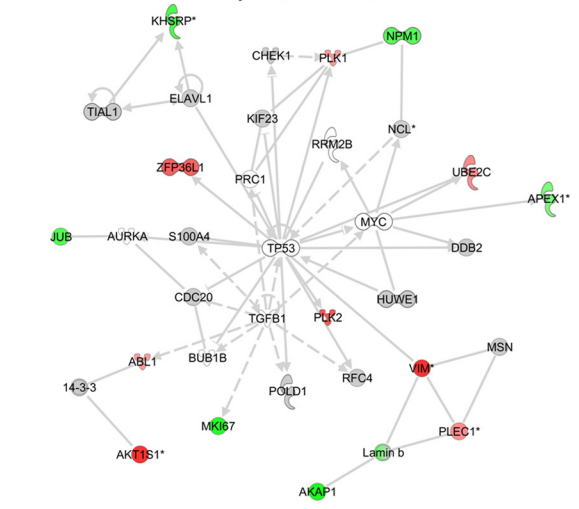

F Network 4: Cellular movement, Cell death, Antigen presentation

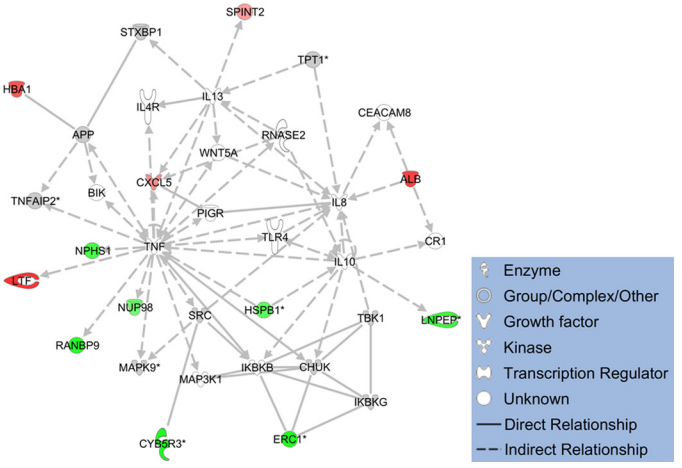

genome wide RNAi screens, mRNA microarray screens, and yeast two-hybrid assay, to identify 1,449 protein targets for further analysis (73). Because viral infection leads to both qualitative and quantitative effects on host gene expression and function, we have complemented these previous studies by deriving a quantitative proteomic assessment of influenza infection to further define the effects of influenza virus infection on host functions. Whereas a variety of quantitative proteomic methods have been employed to examine perturbations in host protein quantities after virus infection, quantification of host protein responses after influenza virus infection had only previously been reported after 2-D DIGE analysis, which identified 25 or fewer proteins (48, 72). Here, we present the application of SILAC and demonstrate several advantages relative to this earlier approach. While 2-D DIGE is excellent for resolving protein species that differ in posttranslational modification, such as phosphorylation, it suffers several drawbacks, including a relatively low dynamic range and sample overloading (13), variability in labeling efficiency, as well as labeling deficits for proteins lacking lysine or cysteine residues, and is unsuited for proteins at the extremes of molecular weight, alkalinity, or hydrophobicity (59). Finally, in-gel digestion methods are usually less efficient in allowing peptide identification than in-solution digestion, which may partially explain why earlier studies identified less than 25 differentially regulated proteins (48, 72).

We used nongel-based quantitative proteomic methods and identified and measured >120,000 SILAC-labeled peptides, which arose from >5,000 host protein pairs. Almost 4,700 cytosolic protein pairs were identified based upon stringent criteria that required two complete L and H tryptic peptides and protein identification confidence of 99% or greater. Of these, statistical tests indicated that 280 proteins (127 upregulated and 153 downregulated) were reliably identified as significantly regulated at the 95% confidence limit. Upregulated proteins included those involved in stress responses, regulation of mRNA transcription, translation initiation, cell structure, molecular binding, and MHC-I-mediated immunity pathways. Downregulated proteins include those involved in alternative splicing, MHC-II-mediated immunity, nucleoside, nucleotide, and nucleic acid metabolism, adhesion, and cytoskeleton regulation. Several proteins (described in more detail below) had been previously described in other studies, but our application of SILAC in combination with multiple purification and fractionation schemes identified more than 10 times as many differentially regulated proteins as have previously been identified in influenza virus infections.

A small number of host proteins have been reported as upregulated by influenza virus infection in earlier quantitative proteomic studies. Keratins, including cytokeratin 10, have repeatedly been shown upregulated as much as 50-fold by A/PR/8/34 infection (3–5, 48, 72). Alterations in these proteins could be expected to have dramatic effects upon intermediate filaments and cellular organization, both of which play significant roles in enveloped virus intracellular transport and budding. However, keratins are also common contaminants in MS experiments, and our Western blot assays suggest that this may have been the case in these studies, as the highly elevated L/H ratios could result from sample contamination with normal unlabeled keratins. This possibility could be tested in follow-up studies by infecting the H-labeled cells, which, if keratins are contaminants, would result in very low L/H ratios. A larger number of genes have been reported affected by influenza virus infection by microarray studies (6, 30). We attempted to correlate our results with these previous transcriptomic analyses and found generally good correlation, as has also been reported in a transcriptomic/semiquantitative proteomic comparison (6). Most of the 22 genes whose products we measured and for which transcriptomic data are readily available correlated well; only 3 were negatively correlated, such that microarrays indicated that STAT3, SNX6, and VIM mRNA levels were upregulated, not affected, and decreased (30), respectively, whereas SILAC indicated that the corresponding proteins were slightly downregulated, upregulated, and highly upregulated, respectively (data not shown).

The myxovirus resistance host proteins Mx1 and Mx2 have been identified as upregulated by influenza infection in several studies, including microarray (30), and in more recent proteomic analyses (6, 72). These interferon (IFN)-induced, large GTPase dynamin-like Mx proteins are important antiviral proteins, particularly against RNA viruses (37, 38). "Semiquantitative" analyses of macaque lungs infected by recombinant influenza virus A/Texas/36/91 (H1N1) suggested an approximate 3-fold upregulation in this protein, and quantitative 2-D DIGE of A549 cells infected with PR8 showed about 5- and 10-fold upregulation at 48 and 72 h postinfection (72). Although MxA (the mouse homolog of Mx1) was apparently not detected at 24 hpi in A549 cells in the earlier study, these values are in good agreement with our measurements of ~5- to 14-fold increases in Mx proteins by PR8 infection in the current study. Vester et al. (72) reported that nucleobindin was upregulated approximately 2-fold by 72 hpi, although it either was not detected or was not upregulated at earlier time points in their study. Our results indicate that nucleobindins were moderately affected but not significantly at 24 hpi (see Table ST-1 in the supplemental material). In addition, Vester et al. reported proteasome activator hPA28 subunit β was also upregulated about 2-fold by 72 hpi, although it either was not

FIG. 5. Molecular pathways of regulated proteins. Proteins and their levels of regulation were imported into the Ingenuity Pathways Analysis (IPA) tool, and interacting pathways were constructed. (A) Overview of 4 networks identified at 95% confidence, each of which contained 10 or more "focus" molecules (molecules significantly up- or downregulated). Each box contains an arbitrary network number (upper) as well as the number of focus molecules within the network (lower bolded number). Lines connecting networks indicate the number of focus molecules present in each attached network. (B) Merged network, containing all molecules present in each of the four individual networks. (C to F) Individual networks with pathway names indicated. Solid lines, direct known interactions; dashed lines, suspected or indirect interactions; red, significantly upregulated proteins; pink, moderately upregulated proteins; gray, proteins identified but not significantly regulated; light green, moderately downregulated proteins; dark green, significantly downregulated proteins; white, proteins known to be in the network but not identified in our study. Molecular classes are indicated in the legends.

detected or was not upregulated at earlier time points in their study. Our results identified a larger number of proteasome-related molecules and indicated that proteasome inhibitor subunit 1 isoform 1 was upregulated about 2.2-fold, proteasome subunit α type 8 was downregulated nearly 3-fold, and numerous other proteasome activators, including PA28β (upregulated 1.2-fold) were only moderately altered at 24 hpi. Reduction in specific host proteins may be mediated by enhanced proteasomal protein production and activity.

Our study identified many more upregulated and downregulated proteins. Notably, some of these have not been reported in previous quantitative influenza virus infections but have been reported as regulated by other viruses. For example, the intermediate filament protein vimentin, seen upregulated to about 7-fold in our study (Table 2), has been reported increased by other negative-sense RNA viruses, including rabies virus (76), and the positive-sense RNA virus hepatitis C (50) but was reported downregulated by West Nile virus (57), HIV (60), infectious bursal disease virus (79), and human papillomavirus type 16 (44). In addition, dermcidin, a sweat gland-produced antibiotic (51, 63) that activates keratinocytes (54) and had been seen upregulated by HIV infection (58), was also upregulated almost 10-fold in our study, suggesting that it may be activated by a broad range of infectious agents. Other notable innate immunity molecules that we found upregulated include IFITM2, B2M, and the ISG15 ubiquitin-like modifier that is involved in IFN-induced inactivation of viral NS1 functions (78).

Most previous quantitative proteomic analyses identified very few influenza virus-induced downregulated proteins. This might be expected because 2-D DIGE is generally limited to analysis of high-abundance proteins (13, 59, 72). This would not be a limitation if barely detectable proteins are upregulated above the detection threshold, but downregulation of barely detectable proteins below the detection limit might preclude their inclusion in the analyses. The downregulated proteins we identified are involved in a very large number of cellular processes (Fig. 4) and include, most notably, those involved in MHC-II mediated immunity, protein folding and modification, nucleoside, nucleotide, and nucleic acid metabolism, adhesion, and cytoskeleton regulation. Several notable proteins were detected and measured multiple times and found to be significantly downregulated. These include β-catenin, found downregulated ~3-fold, a key component of cell adhesion pathways and a target for the ubiquitin proteasome pathway (reviewed in reference 1) that also is involved in regulating lung development (18). Downregulation of the β-catenin protein may avoid IFN induction through the WNT/β-catenin pathway (64). In addition, the WD40 protein, which is involved in signal transduction, molecular binding, particularly with β-catenin, and numerous other processes and is targeted by retroviral insertion (42) and required to aid herpesvirus replication (66), was found downregulated ~100-fold in our study.

Influenza infection is critically dependent on host gene expression because there is a strict requirement for host POL II transcripts as a source of capped oligonucleotides for priming viral transcription, as well as a requirement for splicing machinery to generate NEP and M2 spliced transcripts (reviewed in reference 24). Therefore, influenza virus must maintain and regulate host transcriptional activities to optimize viral replication via the enhanced production of canonical transcription factors, such as TFIIB, TFIIF1, and TFIID7, while downregulating most of the other typical POL II transcription factors. Thus, influenza virus may modulate expression of host POL II transcripts to favor viral replication processes, such as the association of influenza polymerase with POL II early in transcription that may be involved in accessing newly formed capped transcripts as they are produced and concomitantly inhibiting elongation (10, 25). The general transcription factor TFIIA, which regulates RNA POL2-dependent DNA transcription (40), was downregulated ~4-fold. This protein would not be expected to be needed by an RNA virus that uses no DNA intermediates in its replication; however, downregulation of host DNA-dependent transcription could be important for host resistance genes such as IFN and IFN-inducible genes (36). TACC2 (transforming, acidic coiled-coil-containing protein 2 isoform a), a centrosomal-microtubule-associated protein (31) involved in protein translation and RNA processing and transcription (68), was found downregulated >12-fold. Interestingly, this protein is targeted for degradation by SV40 virus (70), suggesting that disparate viruses may benefit from targeting this host protein.

On the other hand, influenza virus has mechanisms for downregulation of gene expression that involve inhibition of polyadenylation through binding of NS1-viral polymerase complexes to cleavage- and polyadenylation-specific factor 30 (47) that serves to block host gene expression. This blocks the expression of host inhibitors, including interferon and tumor necrosis factor alpha (TNF-α) (which were reduced in PR8-infected A549 cells) (Table 3), and thus a balance of host inhibition must be achieved while maintaining host gene transcription of mRNA and protein products employed for replication. Influenza NS1 protein also binds eIF4G1 and PABP1 translation initiation factors to favor influenza protein translation (9, 17, 69) relative to host translation. It is possible that the reduction in eIF4G1 as well as many ribosomal protein components may be involved in the mechanisms for preferential viral gene expression at the expense of host gene expression.

Influenza infection also enhances immune evasion by directing the incorporation of MHC-I into ganglioside-rich microdomains that function to recruit cellular inhibitors of NK cell binding and function (reviewed in reference 14), which is consistent with an upregulation of MHC-I in A549 cells (Table 2; Fig. 4). The downregulation of several components of the MHC-I antigen presentation machinery could also be expected to reduce influenza antigen presentation on the surface of infected cells to result in immune cell-mediated attack. The upregulation of ubiquitin activities as well as the IFN-induced viral antagonist, Mx1, may be an interrelated feature of Mx1 control because Mx1 is found in nuclear promyelocytic leukemia protein (PML) bodies in infected cells that are also sites of ubiquitin degradation (26). We found Mx1 upregulated 14-fold (z-score > 5) in our nuclear fractions, which, as explained earlier, was not further analyzed in the present study (data not shown). With respect to the cytoskeleton components, influenza virus uses actin interactions of NP protein for nucleocytoplasmic transport of RNP (21, 65), and the multiple instances of increases in actins and related components may be instrumental in favoring viral replication. Other upregulated

proteins listed in Table 2 and downregulated proteins listed in Table 3 could be hypothesized to have been affected by infection but will not be discussed further at this time, as they await further validation.

In summary, we have applied SILAC to quantitatively measure the regulation of nearly 4,700 host cytosolic proteins after human A549 lung cells were infected with prototype influenza lab strain A/PR/8/34. Most proteins measured by this nonbiased approach were not substantially altered, having L/H ratios of approximately 1.0. We chose a relatively rigorous statistical cutoff by requiring proteins' z-score values to be >1.96 standard deviation units away from population means, corresponding to 95% confidence. Our study approach was unbiased with respect to any particular groups of proteins because we made no attempt to enrich for any subpopulation of proteins or specific modifications. This study could be extended by analyzing, for example, nuclei of infected cells or phosphorylated proteins. It also will be important to extend these types of analyses to other cell types, including primary airway cells, and to other virus types, including more clinically relevant strains, such as the pandemic H1N1 2009 influenza virus. These types of analyses should identify common, as well as unique, features of each virus-host interaction and may point the way to better-designed antiviral therapies.

ACKNOWLEDGMENTS

This work was supported by grants MT-11630 and PAN-83159 from the Canadian Institutes of Health Research to K.M.C.

We thank Kolawole Opanubi for expert technical assistance, James House, director, Animal Sciences, for embryonated hen eggs in which some influenza virus stocks were grown, Ming Yang for anti-influenza virus NP monoclonal hybridoma cells, and Yoshihiro Kawaoka for the influenza virus reverse genetics system.

K.M.C., D.K., J.W., and E.G.B. designed experiments, K.M.C., A.B., W.X., X.M., and D.K. performed experimental work described herein, O.K. performed mass spectrometry, J.P.C. performed database and computational analyses, and all coauthors edited the manuscript.

The authors declare no conflicts of interest.

REFERENCES

1. **Aberle, H., A. Bauer, J. Stappert, A. Kispert, and R. Kemler.** 1997. Beta-catenin is a target for the ubiquitin-proteasome pathway. EMBO J. **16:**3797–3804.
2. **Alexander, D. J.** 2007. An overview of the epidemiology of avian influenza. Vaccine **25:**5637–5644.
3. **Arcangeletti, M. C., F. De Conto, F. Ferraglia, F. Pinardi, R. Gatti, G. Orlandini, S. Covan, F. Motta, I. Rodighiero, G. Dettori, and C. Chezzi.** 2008. Host-cell-dependent role of actin cytoskeleton during the replication of a human strain of influenza A virus. Arch. Virol. **153:**1209–1221.
4. **Arcangeletti, M. C., F. Pinardi, S. Missorini, F. DeConto, G. Conti, P. Portincasa, K. Scherrer, and C. Chezzi.** 1997. Modification of cytoskeleton and prosome networks in relation to protein synthesis in influenza A virus-infected LLC-MK2 cells. Virus Res. **51:**19–34.
5. **Avalos, R. T., Z. Yu, and D. P. Nayak.** 1997. Association of influenza virus NP and M1 proteins with cellular cytoskeletal elements in influenza virus-infected cells. J. Virol. **71:**2947–2958.
6. **Baas, T., C. R. Baskin, D. L. Diamond, A. Garcia-Sastre, H. Bielefeldt-Ohmann, T. M. Tumpey, M. J. Thomas, V. S. Carter, T. H. Teal, N. Van Hoeven, S. Proll, J. M. Jacobs, Z. R. Caldwelll, M. A. Gritsenko, R. R. Hukkanen, D. G. Camp, R. D. Smith, and M. G. Katze.** 2006. Integrated molecular signature of disease: analysis of influenza virus-infected macaques through functional genomics and proteomics. J. Virol. **80:**10813–10828.
7. **Bonaldi, T., T. Straub, J. Cox, C. Kumar, P. B. Becker, and M. Mann.** 2008. Combined use of RNAi and quantitative proteomics to study gene function in Drosophila. Mol. Cell **31:**762–772.
8. **Brown, E. G.** 1990. Increased virulence of a mouse-adapted variant of influenza A/Fm/1/47 virus is controlled by mutations in genome segments 4, 5, 7, and 8. J. Virol. **64:**4523–4533.
9. **Burgui, I., T. Aragon, J. Ortin, and A. Nieto.** 2003. PABP1 and eIF4Gl associate with influenza virus NS1 protein in viral mRNA translation initiation complexes. J. Gen. Virol. **84:**3263–3274.
10. **Chan, A. Y., F. T. Vreede, M. Smith, O. G. Engelhardt, and E. Fodor.** 2006. Influenza virus inhibits RNA polymerase II elongation. Virology **351:**210–217.
11. **Chen, R., S. Pan, R. Aebersold, and T. A. Brentnall.** 2007. Proteomics studies of pancreatic cancer. Proteomics Clin. Appl. **1:**1582–1591.
12. **Choe, L. H., K. Aggarwal, Z. Franck, and K. H. Lee.** 2005. A comparison of the consistency of proteome quantitation using two-dimensional electrophoresis and shotgun isobaric tagging in Escherichia coli cells. Electrophoresis **26:**2437–2449.
13. **Corthals, G. L., V. C. Wasinger, D. F. Hochstrasser, and J. C. Sanchez.** 2000. The dynamic range of protein expression: a challenge for proteomic research. Electrophoresis **21:**1104–1115.
14. **Culley, F. J.** 2009. Natural killer cells in infection and inflammation of the lung. Immunology **128:**151–163.
15. **de Godoy, L. M. F., J. V. Olsen, J. Cox, M. L. Nielsen, N. C. Hubner, F. Frohlich, T. C. Walther, and M. Mann.** 2008. Comprehensive mass-spectrometry-based proteome quantification of haploid versus diploid yeast. Nature **455:**1251–1254.
16. **de Hoog, C. L., L. J. Foster, and M. Mann.** 2004. RNA and RNA binding proteins participate in early stages of cell spreading through spreading initiation centers. Cell **117:**649–662.
17. **de la Luna, S., P. Fortes, A. Beloso, and J. Ortin.** 1995. Influenza virus NS1 protein enhances the rate of translation initiation of viral mRNAs. J. Virol. **69:**2427–2433.
18. **De Langhe, S. P., G. Carraro, D. Tefft, C. G. Li, X. Xu, Y. Chai, P. Minoo, M. K. Hajihosseini, J. Drouin, V. Kaartinen, and S. Bellusci.** 2008. Formation and differentiation of multiple mesenchymal lineages during lung development is regulated by beta-catenin signaling. PLoS One **3:**e1516–PMID18231602.
19. **Dennis, G., B. T. Sherman, D. A. Hosack, J. Yang, W. Gao, H. C. Lane, and R. A. Lempicki.** 2003. DAVID: database for annotation, visualization, and integrated discovery. Genome Biol. **4:**R60.
20. **DeSouza, L., G. Diehl, M. J. Rodrigues, J. Z. Guo, A. D. Romaschin, T. J. Colgan, and K. W. M. Siu.** 2005. Search for cancer markers from endometrial tissues using differentially labeled tags iTRAQ and clCAT with multidimensional liquid chromatography and tandem mass spectrometry. J. Proteome Res. **4:**377–386.
21. **Digard, P., D. Elton, K. Bishop, E. Medcalf, A. Weeds, and B. Pope.** 1999. Modulation of nuclear localization of the influenza virus nucleoprotein through interaction with actin filaments. J. Virol. **73:**2222–2231.
22. **Dwivedi, R. C., V. Spicer, M. Harder, M. Antonovici, W. Ens, K. G. Standing, J. A. Wilkins, and O. V. Krokhin.** 2008. Practical implementation of 2D HPLC scheme with accurate peptide retention prediction in both dimensions for high-throughput bottom-up proteomics. Anal. Chem. **80:**7036–7042.
23. **Elliott, M. H., D. S. Smith, C. E. Parker, and C. Borchers.** 2009. Current trends in quantitative proteomics. J. Mass Spectrom. **44:**1637–1660.
24. **Engelhardt, O. G., and E. Fodor.** 2006. Functional association between viral and cellular transcription during influenza virus infection. Rev. Med. Virol. **16:**329–345.
25. **Engelhardt, O. G., M. Smith, and E. Fodor.** 2005. Association of the influenza a virus RNA-dependent RNA polymerase with cellular RNA polymerase II. J. Virol. **79:**5812–5818.
26. **Engelhardt, O. G., E. Ullrich, G. Kochs, and O. Haller.** 2001. Interferon-induced antiviral Mx1 GTPase is associated with components of the SUMO-1 system and promyelocytic leukemia protein nuclear bodies. Exp. Cell Res. **271:**286–295.
27. **Everley, P. A., J. Krijgsveld, B. R. Zetter, and S. P. Gygi.** 2004. Quantitative cancer proteomics: stable isotope labeling with amino acids in cell culture (SILAC) as a tool for prostate cancer research. Mol. Cell. Proteomics **3:**729–735.
28. **Feinberg, A. P.** 2007. Phenotypic plasticity and the epigenetics of human disease. Nature **447:**433–440.
29. **Garcia-Ramirez, M., F. Canals, C. Hernandez, N. Colome, C. Ferrer, E. Carrasco, J. Garcia-Arumi, and R. Simo.** 2007. Proteomic analysis of human vitreous fluid by fluorescence-based difference gel electrophoresis (DIGE): a new strategy for identifying potential candidates in the pathogenesis of proliferative diabetic retinopathy. Diabetologia **50:**1294–1303.
30. **Geiss, G. K., M. Salvatore, T. M. Tumpey, V. S. Carter, X. Y. Wang, C. F. Basler, J. K. Taubenberger, R. E. Bumgarner, P. Palese, M. G. Katze, and A. Garcia-Sastre.** 2002. Cellular transcriptional profiling in influenza A virus-infected lung epithelial cells: the role of the nonstructural NS1 protein in the evasion of the host innate defense and its potential contribution to pandemic influenza. Proc. Natl. Acad. Sci. U. S. A. **99:**10736–10741.
31. **Gergely, F., C. Karlsson, I. Still, J. Cowell, J. Kilmartin, and J. W. Raff.** 2000. The TACC domain identifies a family of centrosomal proteins that can interact with microtubules. Proc. Natl. Acad. Sci. U. S. A. **97:**14352–14357.
32. **Gilar, M., P. Olivova, A. E. Daly, and J. C. Gebler.** 2005. Orthogonality of separation in two-dimensional liquid chromatography. Anal. Chem. **77:**6426–6434.
33. **Goldberg, A. D., C. D. Allis, and E. Bernstein.** 2007. Epigenetics: a landscape takes shape. Cell **128:**635–638.
34. **Graumann, J., N. C. Hubner, J. B. Kim, K. Ko, M. Moser, C. Kumar, J. Cox,**

H. Scholer, and M. Mann. 2008. Stable isotope labeling by amino acids in cell culture (SILAC) and proteome quantitation of mouse embryonic stem cells to a depth of 5,111 proteins. Mol. Cell. Proteomics **7:**672–683.
35. **Gygi, S. P., B. Rist, S. A. Gerber, F. Turecek, M. H. Gelb, and R. Aebersold.** 1999. Quantitative analysis of complex protein mixtures using isotope-coded affinity tags. Nat. Biotechnol. **17:**994–999.
36. **Hale, B. G., R. E. Randall, J. Ortin, and D. Jackson.** 2008. The multifunctional NS1 protein of influenza A viruses. J. Gen. Virol. **89:**2359–2376.
37. **Haller, O., and G. Kochs.** 2002. Interferon-induced mx proteins: dynamin-like GTPases with antiviral activity. Traffic **3:**710–717.
38. **Haller, O., P. Staeheli, and G. Kochs.** 2009. Protective role of interferon-induced Mx GTPases against influenza viruses. Rev. Sci. Tech. **28:**219–231.
39. **Han, D. K., J. Eng., H. L. Zhou, and R. Aebersold.** 2001. Quantitative profiling of differentiation-induced microsomal proteins using isotope-coded affinity tags and mass spectrometry. Nat. Biotechnol. **19:**946–951.
40. **Hoiby, T., H. Q. Zhou, D. J. Mitsiou, and H. G. Stunnenberg.** 2007. A facelift for the general transcription factor TFIIA. Biochim. Biophys. Acta **1769:**429–436.
41. **Huang, D. W., B. T. Sherman, and R. A. Lempicki.** 2009. Systematic and integrative analysis of large gene lists using DAVID bioinformatics resources. Nat. Protoc. **4:**44–57.
42. **Jiang, X. Y., Z. Hanna, M. Kaouass, L. Girard, and P. Jolicoeur.** 2002. Ahi-1, a novel gene encoding a modular protein with WD40-repeat and SH3 domains, is targeted by the Ahi-1 and Mis-2 provirus integrations. J. Virol. **76:**9046–9059.
43. **Keshamouni, V. G., P. Jagtap, G. Michailidis, J. R. Strahler, R. Kuick, A. K. Reka, P. Papoulias, R. Krishnapuram, A. Srirangam, T. J. Standiford, P. C. Andrews, and G. S. Omenn.** 2009. Temporal quantitative proteomics by iTRAQ 2D-LC-MS/MS and corresponding mRNA expression analysis identify posttranscriptional modulation of actin-cytoskeleton regulators during TGF-beta-induced epithelial-mesenchymal transition. J. Proteome Res. **8:**35–47.
44. **Kim, E., J. Kang, M. Cho, S. Lee, E. Seo, H. Choi, Y. Kim, J. Kim, K. Y. Kang, K. P. Kim, J. Han, Y. Sheen, Y. N. Yum, S. N. Park, and D. Y. Yoon.** 2009. Profiling of transcripts and proteins modulated by the E7 oncogene in the lung tissue of E7-Tg mice by the omics approach. Mol. Med. Rep. **2:**129–137.
45. **Kobasa, D., S. M. Jones, K. Shinya, J. C. Kash, J. Copps, H. Ebihara, Y. Hatta, J. H. Kim, P. Halfmann, M. Hatta, F. Feldmann, J. B. Alimonti, L. Fernando, Y. Li, M. G. Katze, H. Feldmann, and Y. Kawaoka.** 2007. Aberrant innate immune response in lethal infection of macaques with the 1918 influenza virus. Nature **445:**319–323.
46. **Krauss, S., C. A. Obert, J. Franks, D. Walker, K. Jones, P. Seiler, L. Niles, S. P. Pryor, J. C. Obenauer, C. W. Naeve, L. Widjaja, R. J. Webby, and R. G. Webster.** 2007. Influenza in migratory birds and evidence of limited intercontinental virus exchange. PLoS Pathog. **3:**1684–1693.
47. **Kuo, R. L., and R. M. Krug.** 2009. Influenza A virus polymerase is an integral component of the CPSF30-NS1A protein complex in infected cells. J. Virol. **83:**1611–1616.
48. **Liu, N., W. J. Song, P. Wang, K. C. Lee, W. Chan, H. L. Chen, and Z. W. Cai.** 2008. Proteomics analysis of differential expression of cellular proteins in response to avian H9N2 virus infection in human cells. Proteomics **8:**1851–1858.
49. **Lucitt, M. B., T. S. Price, A. Pizarro, W. Wu, A. K. Yocum, C. Seiler, M. A. Pack, I. A. Blair, G. A. FitzGerald, and T. Grosser.** 2008. Analysis of the zebrafish proteome during embryonic development. Mol. Cell. Proteomics **7:**981–994.
50. **Matos, J. M., F. A. Witzmann, O. W. Cummings, and C. M. Schmidt.** 2009. A pilot study of proteomic profiles of human hepatocellular carcinoma in the United States. J. Surg. Res. **155:**237–243.
51. **Murakami, M., T. Ohtake, R. A. Dorschner, B. Schittek, C. Garbe, and R. L. Gallo.** 2002. Cathelicidin anti-microbial peptide expression in sweat, an innate defense system for the skin. J. Invest. Dermatol. **119:**1090–1095.
52. **Nesvizhskii, A. I., and R. Aebersold.** 2005. Interpretation of shotgun proteomic data: the protein inference problem. Mol. Cell. Proteomics **4:**1419–1440.
53. **Neumann, G., T. Watanabe, H. Ito, S. Watanabe, H. Goto, P. Gao, M. Hughes, D. R. Perez, R. Donis, E. Hoffmann, G. Hobom, and Y. Kawaoka.** 1999. Generation of influenza A viruses entirely from cloned cDNAs. Proc. Natl. Acad. Sci. U. S. A. **96:**9345–9350.
54. **Niyonsaba, F., A. Suzuki, H. Ushio, I. Nagaoka, H. Ogawa, and K. Okumura.** 2009. The human antimicrobial peptide dermcidin activates normal human keratinocytes. Br. J. Dermatol. **160:**243–249.
55. **Ong, S. E., and M. Mann.** 2005. Mass spectrometry-based proteomics turns quantitative. Nat. Cell Biol. **1:**252–262.
56. **Palese, P., and M. L. Shaw.** 2007. Orthomyxoviridae: the viruses and their replication, p. 1647–1689. *In* D. M. Knipe and P. M. Howley (ed.), Fields virology. Lippincott Williams & Wilkins, Philadelphia, PA.
57. **Pastorino, B., E. Boucomont-Chapeaublanc, C. N. Peyrefitte, M. Belghazi, T. Fusai, C. Rogier, H. J. Tolou, and L. Almeras.** 2009. Identification of cellular proteome modifications in response to West Nile virus infection. Mol. Cell. Proteomics **8:**1623–1637.
58. **Pathak, S., G. A. De Souza, T. Salte, H. G. Wiker, and B. Asjo.** 2009. HIV induces both a down-regulation of IRAK-4 that impairs TLR signalling and an up-regulation of the antibiotic peptide dermcidin in monocytic cells. Scand. J. Immunol. **70:**264–276.
59. **Patton, W. F.** 2002. Detection technologies in proteome analysis. J. Chromatogr. B Analyt. Technol. Biomed. Life Sci. **771:**3–31.
60. **Pocernich, C. B., D. Boyd-Kimball, H. F. Poon, V. Thongboonkerd, B. C. Lynn, J. B. Klein, V. Calebrese, A. Nath, and D. A. Butterfield.** 2005. Proteomics analysis of human astrocytes expressing the HIV protein Tat. Mol. Brain Res. **133:**307–316.
61. **Prange, A., and D. Proefrock.** 2008. Chemical labels and natural element tags for the quantitative analysis of bio-molecules. J. Anal. Atomic Spectrom. **23:**432–459.
62. **Prokhorova, T. A., K. T. G. Rigbolt, P. T. Johansen, J. Henningsen, I. Kratchmarova, M. Kassem, and B. Blagoev.** 2009. Stable isotope labeling by amino acids in cell culture (SILAC) and quantitative comparison of the membrane proteomes of self-renewing and differentiating human embryonic stem cells. Mol. Cell. Proteomics **8:**959–970.
63. **Schittek, B., R. Hipfel, B. Sauer, J. Bauer, H. Kalbacher, S. Stevanovic, M. Schirle, K. Schroeder, N. Blin, F. Meier, G. Rassner, and C. Garbe.** 2001. Dermcidin: a novel human antibiotic peptide secreted by sweat glands. Nat. Immunol. **2:**1133–1137.
64. **Shapira, S. D., I. Gat-Viks, B. O. V. Shum, A. Dricot, M. M. de Grace, L. G. Wu, P. B. Gupta, T. Hao, S. J. Silver, D. E. Root, D. E. Hill, A. Regev, and N. Hacohen.** 2009. A physical and regulatory map of host-influenza interactions reveals pathways in H1N1 infection. Cell **139:**1255–1267.
65. **Simpson-Holley, M., D. Ellis, D. Fisher, D. Elton, J. McCauley, and P. Digard.** 2002. A functional link between the actin cytoskeleton and lipid rafts during budding of filamentous influenza virions. Virology **301:**212–225.
66. **Smith, C. C., J. Nelson, L. Aurelian, M. Gober, and B. B. Goswami.** 2000. Ras-GAP binding and phosphorylation by herpes simplex virus type 2 RR1 PK (ICP10) and activation of the Ras/MEK/MAPK mitogenic pathway are required for timely onset of virus growth. J. Virol. **74:**10417–10429.
67. **Spicer, V., A. Yamchuk, J. Cortens, S. Sousa, W. Ens, K. G. Standing, J. A. Wilkins, and O. Krokhin.** 2007. Sequence-specific retention calculator. A family of peptide retention time prediction algorithms in reversed-phase HPLC: applicability to various chromatographic conditions and columns. Anal. Chem. **79:**8762–8768.
68. **Still, I. H., A. K. Vettaikkorumakankauv, A. DiMatteo, and P. Liang.** 2004. Structure-function evolution of the transforming acidic coiled coil genes revealed by analysis of phylogenetically diverse organisms. BMC Evol. Biol. **4:**16.
69. **Taubenberger, J. K.** 2003. Fixed and frozen flu: the 1918 influenza and lessons for the future. Avian Dis. **47:**789–791.
70. **Tei, S., N. Saitoh, T. Funahara, S. Iida, Y. Nakatsu, K. Kinoshita, Y. Kinoshita, H. Saya, and M. Nakao.** 2009. Simian virus 40 large T antigen targets the microtubule-stabilizing protein TACC2. J. Cell Sci. **122:**3190–3198.
71. **Tian, Q., S. B. Stepaniants, M. Mao, L. Weng, M. C. Feetham, M. J. Doyle, E. C. Yi, H. Y. Dai, V. Thorsson, J. Eng., D. Goodlett, J. P. Berger, B. Gunter, P. S. Linseley, R. B. Stoughton, R. Aebersold, S. J. Collins, W. A. Hanlon, and L. E. Hood.** 2004. Integrated genomic and proteomic analyses of gene expression in mammalian cells. Mol. Cell. Proteomics **3:**960–969.
72. **Vester, D., E. Rapp, D. Gade, Y. Genzel, and U. Reichl.** 2009. Quantitative analysis of cellular proteome alterations in human influenza A virus-infected mammalian cell lines. Proteomics **9:**3316–3327.
73. **Watanabe, T., S. Watanabe, and Y. Kawaoka.** 2010. Cellular networks involved in the influenza virus life cycle. Cell Host Microbe **7:**427–439.
74. **Yang, M., Y. Berhane, T. Salo, M. Li, K. Hole, and A. Clavijo.** 2008. Development and application of monoclonal antibodies against avian influenza virus nucleoprotein. J. Virol. Methods **147:**265–274.
75. **Yates, J. R., C. I. Ruse, and A. Nakorchevsky.** 2009. Proteomics by mass spectrometry: approaches, advances, and applications. Annu. Rev. Biomed. Eng. **11:**49–79.
76. **Zandi, F., N. Eslami, M. Soheili, A. Fayaz, A. Gholami, and B. Vaziri.** 2009. Proteomics analysis of BHK-21 cells infected with a fixed strain of rabies virus. Proteomics **9:**2399–2407.
77. **Zhang, Y., A. Wolf-Yadlin, P. L. Ross, D. J. Pappin, J. Rush, D. A. Lauffenburger, and F. M. White.** 2005. Time-resolved mass spectrometry of tyrosine phosphorylation sites in the epidermal growth factor receptor signaling network reveals dynamic modules. Mol. Cell. Proteomics **4:**1240–1250.
78. **Zhao, C., T. Y. Hsiang, R. L. Kuo, and R. M. Krug.** 2010. ISG15 conjugation system targets the viral NS1 protein in influenza A virus-infected cells. Proc. Natl. Acad. Sci. U. S. A. **107:**2253–2258.
79. **Zheng, X. J., L. L. Hong, L. X. Shi, J. Q. Guo, Z. Sun, and J. Y. Zhou.** 2008. Proteomics analysis of host cells infected with infectious bursal disease virus. Mol. Cell. Proteomics **7:**612–625.